# In-situ compaction measurements using gamma ray markers

By Pepijn Kole, NAM
Document number: EP201506209302

## 1 Introduction and objectives

The main aim of the current study of the in-situ compaction data is to improve the spatial/temporal resolution of the analysis, such that the data can help in evaluating the time-dependent compaction models. The accuracy of the analysis that is currently quoted ranges from 1-5mm per marker interval. The Groningen compaction rate is roughly 10mm/year over the full reservoir height, which equates to about 0.6mm/year per marker interval (intervals being ~10m), meaning that every 3-5years (present survey cycle time) the compaction per marker interval is expected to be around 2-3mm, i.e. within the current accuracy. One could simply increase the survey cycle time and argue that over longer times the method is still accurate, however that way subtle changes in compaction rates, like those expected in time decay and multi-rate models, cannot be detected over shorter time scales. Instead of increasing the survey cycle time, we investigate possibilities of improving the analysis accuracy.

Additionally, we aim to refine the intervals over which compaction is determined. The currently reported compaction rates determined from the data are averages over the full reservoir, where poorly interpretable marker intervals were ignored and the compaction over the more reliable intervals were added up. Instead of generalizing the compaction over the full reservoir height, an improved spatial resolution and improved reliability of each marker interval can help make it possible to determine the compaction per marker interval individually. The refinement in turn makes it possible to compare the compaction rates for reservoir properties and characteristics such as porosity, gas/water fill, lower/upper Slochteren, etc, which has all been 'averaged out' in the existing analysis. Correlating the compaction rates with reservoir properties can help make the compaction and subsidence models more realistic. Moreover, the compressibility, $C_m$, can be determined more accurately after the refinement, as the interval's pressure depletion from the reservoir models can be used instead of the reservoir's average.

One must note that the accuracy of existing analysis methods of the in-situ compaction data is already high given the nature of the signals, and still serves its purpose in most reservoirs with high compaction rates. To look at small changes and subtle details of the compaction, however, we want to improve the resolution as much as possible to be able to obtain as much detail and information as we can get from the historic data.

Figure 1 helps visualise the already high accuracy of the existing methods, given the types of signals we are dealing with. A typical measured gamma ray spectrum is shown, displaying a very broad marker intensity peak. Later on, we show that the widths of these peaks are inherent to the technique of using markers inside the formation, and hence the widths cannot be reduced by

improving equipment. On top of the signal in Figure 1  we plotted lines to highlight a +/-5mm and +/-1mm interval, being much smaller than the widths of these peaks. To measure the compaction, the interval length between two of these peaks, approximately 10m apart, needs to be determined, both of which have a similar uncertainty. Inferring a compaction on the order of millimetres seems hence difficult from these data, especially when keeping wireline tool motion in mind. However, with the current and improved analysis methods, we will demonstrate to be able to be near the millimetre accuracy, if measurement conditions are optimal.

Note that GR markers have only been installed in wells in the Groningen field (plus some peripheral wells). The monitoring of in-situ compaction can therefore only be done for the Groningen field, and the outcome can at best serve as an analogue for other fields.
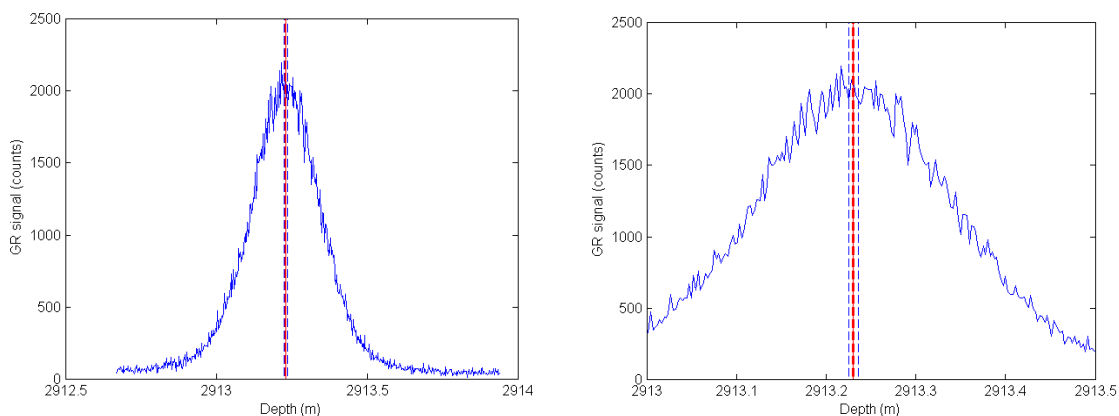


Figure 1: Illustrating the high level of accuracy. Real peak as measured by a CMI tool (Baker Hughes) in well Stedum-1, right same data but zoomed in. Blue lines show mean peak +/- 5mm, red lines +/- 1mm.

## 1.1   Report outline

First, we give a background to the data acquisition and the wells where these GM markers have been installed.  Then, we describe the current analysis method and propose two improvements (one fit method and a cross correlation method) to the data processing for more accurate marker separation determination. These methods are tested through simulation of signals similar to those measured in the field. Finally, we apply the new cross correlation method to the historic data of the SDM-1 well.

An overview of existing data that can be re-interpreted for all the wells is given in the appendix.

## 2   Background of in-situ compaction monitoring in the Groningen field

For a detailed overview of the wells and history of the in-situ compaction measurements, please refer to [1] for an overview of the application in the Groningen field from 1994, and [2] for a more recent review (2002), giving a generic overview of the technique and its history, and it use demonstrated through various field examples.

In and around the Groningen field, GR markers ($^{137}$Cs) have been placed at regular intervals in a number of wells for compaction monitoring. The tools that have been used throughout the years are Precise Depth Measurement (PDM, Schlumberger), Formation Subsidence Measurement Tool (FSMT, Schlumberger) and Compaction Measurement Instrument (CMI, Baker Hughes). The PDM was the first tool, which was run from 1971 to 1982, when it was replaced by the FSMT. The CMI was tested in Ten Boer-4 in 1996 and in Stedum-1 in 1997, and replaced the FSMT in 2010.

An overview of the wells with GR markers is given in Table 1, and their locations in the field shown in Figure 2. The wells that were found to give the most accurate results were Stedum-1, Roode Til-1A and De Hond-1. Results from surveys in Uithuizenmeeden, Schildmeer, Ten Boer and Delfzijl were deemed to be less [3]. Sticking problems in Schaaphok were such that all measurements were deemed unreliable, hence the Schaaphok well has not been surveyed since 1985. Sappermeer was lost due to mechanical failure. The wells Usquert-1 and Bierum-1 have been recompleted as producing wells. De Hond-1 was found to have a broken side-wall entry valve in 2014, making future surveys unlikely. The last survey in De Hond-1 was in 2009.
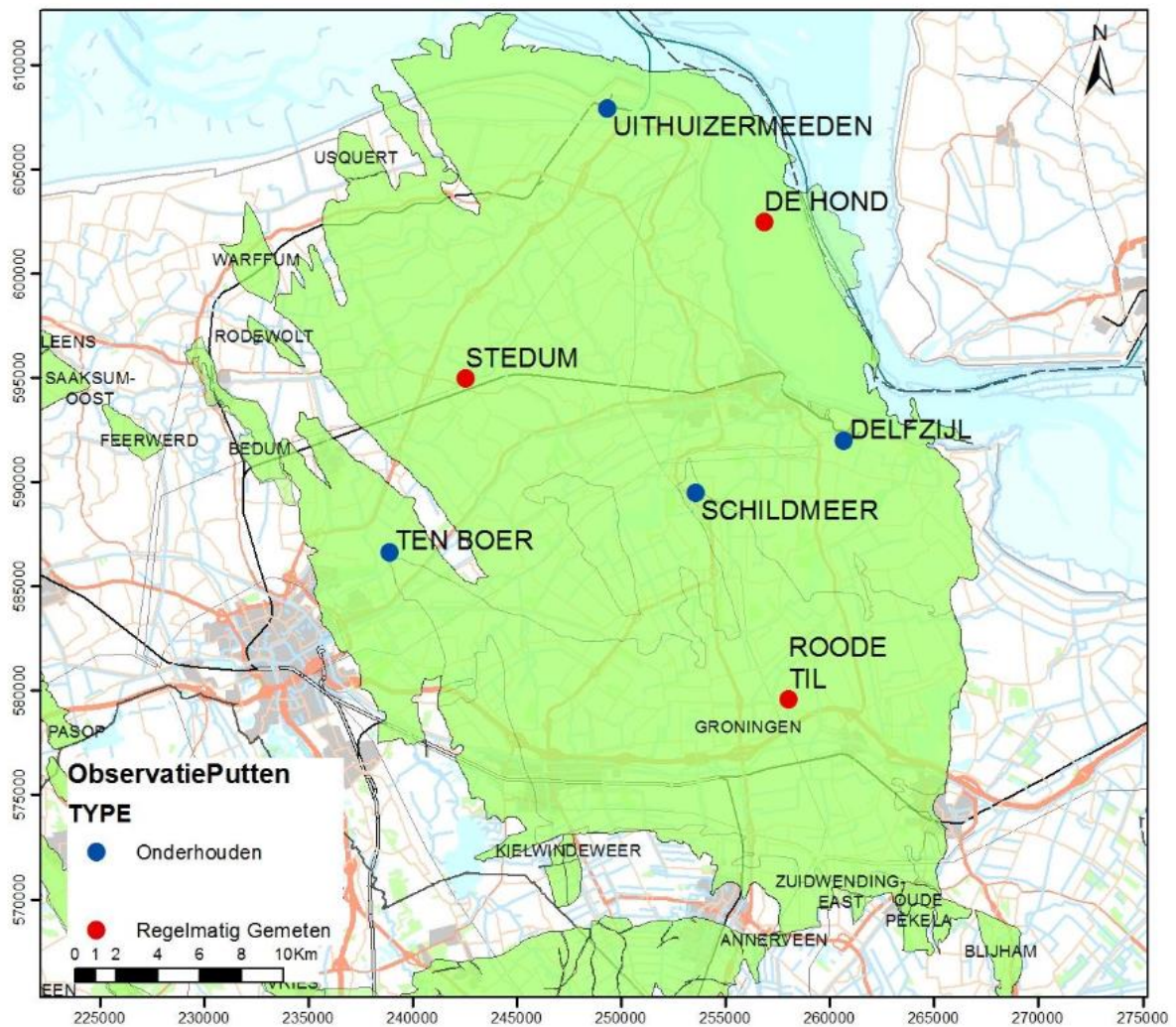


Figure 2: Locations of wells in and around the Groningen field that have GR markers installed. Figure reproduced from [9]

**Table 1: Wells with GR markers for compaction monitoring**

| Well | Coverage (m) | Approximate interval length (m) | Covered zones | Last survey | Comment |
|---|---|---|---|---|---|
| Schaaphok | 160 | 10 | RO | 1985 | Significant sticking problems → discontinued surveys from 1985 |
| Sappemeer | 190 | | RO, DC | | Mechanical issues |
| Uithuizenmeeden | 340 | 12.5 | RO, DC | 1997 | |
| Schildmeer | 160 | 10 | RO | 1996 | |
| Delfzijl | 150 | 10 | RO | 1995 | |
| De Hond | 370 | 10 | RO, DC | 2009 | Might be abandoned, no more logging possible (only during abandonment) |
| Stedum | 210 | 5, 10 | RO | 2013 | |
| Ten Boer | 300 | 10 | ROCLT, RO, DC | 1999 | |
| Roode Til | 1520 | 3?, 10 | CK, KN, RB, ZE, RO, DC | 2011 | |
| Bierum | 150 | | RO | | Producer |
| Usquert | 600 | 10 | ZE, RO, DC | | Producer |

# 3   Analysis methods

Here we describe the different methods used to analyse the GR marker data. The historically applied methods, performed by the logging contractors, will be discussed first, followed by an improved way of determining the marker locations, and the introduction of a new method that employs cross correlations for determining marker separations directly, rather than determining individual marker locations.

## 3.1   Description of historic analysis methods

All CMI data has been processed and analysed by Baker Hughes, who reported all the compaction rates from these CMI logs. Their method is described in detail in [4], here we briefly outline the process. Schlumberger applies a very similar method [5], we highlight the differences below.

The method finds the location of each GR marker and looks at the distance between these peaks directly. To reduce the uncertainty due to tool motion, the tools have multiple detectors with more or less known separation between them. Figure 3 is a schematic of the signals from three GR markers as measured by two different detectors (green and blue lines), as a function of depth. The intensity peaks correspond to different GR markers, which are labelled (1), (2) and (3) in the illustration. The depth is referenced to the depth of one detector (or top of tool string), hence there is a depth shift between the signals from the different detectors, indicated by the separation $L_{Det1-Det2}$ in the figure. One measurement of the separation between markers (1) and (2), $L_{GR1-GR2}$, would be the distance between the corresponding peaks in the signal, as indicated in the illustration for the green detector.

To reduce the depth uncertainty over longer length scales, resulting from for example stick-slip, one can also deduce the marker separation from comparing the location of marker (1) in the green detector signal, with the location of marker (2) in the blue detector signal, which are recorded at a much shorter tool movement and hence are expected to have a reduced depth uncertainty between them. The detector separation must be known accurately to perform this analysis. The tools are designed to have some detector spacings to be almost equal to the marker separation, in which case the two recorded peaks, (1) in green and (2) in blue, would almost occur at the same depth.

Both the CMI and FSMT tools have four detectors, resulting in a total of 10 separations determined for every GR marker pair from each logging run. These can be compared, and outlier values are removed from the analysis.

The most important part for the analysis is finding the positions for each peak in each detector readings as a function of depth. In finding the peak locations, the method applied to the CMI data first cleans the response from each marker by a Gaussian filter. The exact details of the filtering are not disclosed, but from the supplied data, it seems the data in Fourier space is multiplied by a Gaussian peak, which is similar as convoluting the real space signal with the Fourier transform of that filter Gaussian. According to the documentation, the Gaussian in real space is of similar width to the measured signals. The Fourier-type filtering applied has two effects on the raw signal: 1) it will 'remove' noise, in that the output curve will look smoother, and 2) it will broaden the peak signals. An example from their paper is shown in Figure 4 below. The Schlumberger method is very similar, in that they apply a moving-average filtering, which is essentially a convolution with a top-hat function instead of the Gaussian shape applied by Baker Hughes.
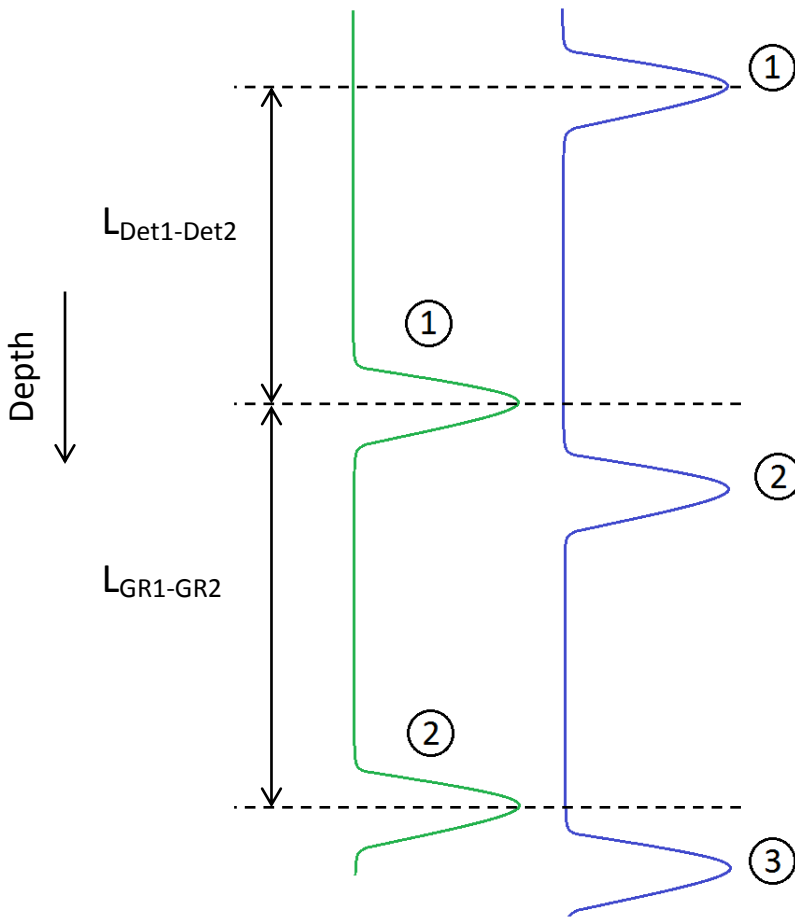
**Figure 3: Schematic of GR marker signals as measured by two detectors on a logging tool, as a function of depth. Signal from one detector plotted in green, the other in blue. Peaks from individual GR markers are labelled (1), (2), (3).**
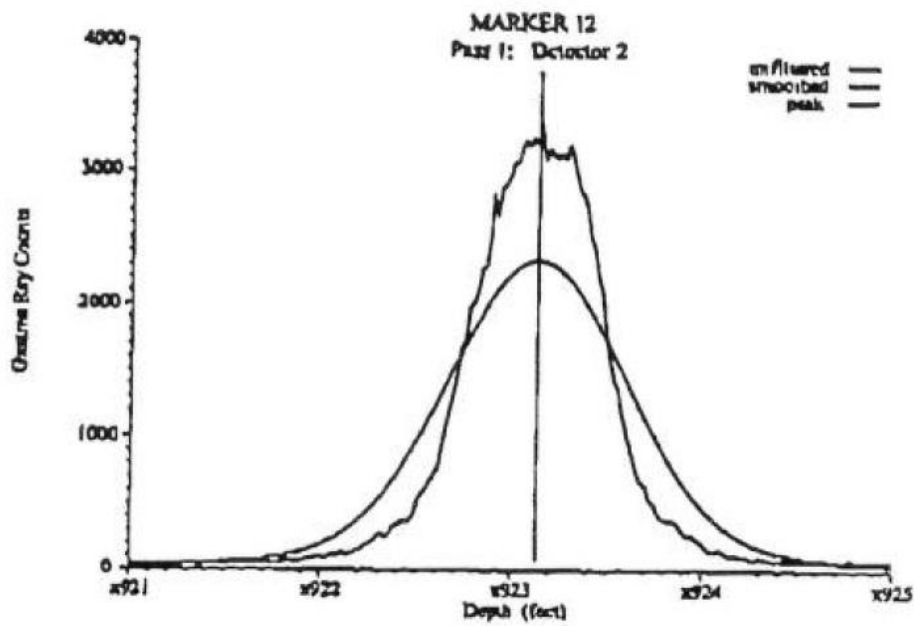


**Figure 4: Example from [4] of a marker signal in raw data and after filtering. The data after filtering shows a much smoother peak, however also a much wider peak.**

After the filtering has been performed, a third order polynomial ($f(x) = ax^3+bx^2+cx+d$) is fitted to the 9 data points in the centre of the filtered signal, using a least-squares method. The derivative of the function is set to equal zero, and from the two resulting solutions for $x$, the one giving a positive value of $f(x)$ is selected to be the central position of the peak.

A problem with the Baker method is that a smoothing filter, or a windowing filter in Fourier space, is used. Such a filter does change the functional shape of the signal, most notably the width of peaks, as is visible in Figure 4. The transformation of the shape is symmetrical; therefore if the original signal is symmetrical the resulting transformation should also be symmetrical, preserving peak positions. If the input signal is however not symmetrical, the signal after filtering will be altered asymmetrically and peak positions are not necessarily preserved. As asymmetries can arise from many sources (cable speed, tool response function, gamma ray source, inhomogeneity of absorption and/or natural formation radiation, etc), it is likely that subtle asymmetries are present in the peaks.

Additionally, the error quoted in the analysis seems to be underestimating the actual uncertainty in the interpretation of the peak separation. The errors are estimated from the empirical relation [4]:

$$\sigma_{peak} = 0.511\sqrt{\frac{\Delta z \cdot FWHM}{n}}$$

Here, $\Delta z$ is the distance between data samples (about 5-6mm for CMI data), $FWHM$ is the full width at half maximum (not explained if it is the FWHM of the raw or filtered signal) and $n$ is the number of counts in the peak (again, not explained if it is for the raw or filtered signal). The equation does not include signal qualities such as signal to noise, and assumes that the shape of the peak can be approximated as Gaussian; deviations from this are not included in the uncertainty. It also assumes the noise behaves like shot noise, but when looking at the noise of measured signals, these commonly exceed the *sqrt(n)* level by a factor of 2. Unfortunately, the reference frequently quoted for directing to an explanation of the empirical relation, seems to have not been published to date [6].

The typical uncertainties resulting from the above equation ($\Delta z$ = 6mm, $FWHM$ = 300mm, $n$ > 1000counts) are less than 1mm, whereas the data point separation in the data is already 6mm. As their method does not apply any interpolation in between data points apart from obtaining the maximum of the polynomial fitted to the filtered signal, it is unlikely that their accuracy is significantly less than the data point separation. Moreover, the method assumes perfectly sampled signals and can only mark results as unreliable (e.g. resulting from stick-slip) if the outcome differs too much from other results.

## 3.2   Improved traditional method

The Baker method seems to be optimised for low computing power, which was important in the early days of the in-situ compaction measurements. It must be noted that it still provides an output accurate enough for high-rate compaction and for determining the long-term compaction for a field like Groningen, but it cannot be applied to study small compaction rates and small variations.

An improvement to the method would be to fit a peak function, like a Gaussian or Lorentzian, to the peaks as they are measured without altering the signals first via filters. Such a method will look at the function al shape of the whole peak, and use many more data points to determine a best centre of the peak. The noise and deviations from a perfect Gaussian will result in some uncertainty, obtained by the fit method itself, which can be used as a more accurate measure of the error in the output values.

Nowadays, such fit routines can easily be implemented in software like Matlab, so we will not discuss the details here further.

## 3.3 New cross correlation method

Besides improving the determination of the peak locations by applying a standard fit routine, we also present a new analysis method that works through cross correlation of signals. The advantages of cross correlations in these types of measurement are that random noises like those observed here will cancel out in the process, resulting in a smooth output signal that only holds information of the correlation between two signals on different length scales. When looking at the signals in the illustration of Figure 3, the length scales over which there is correlation between the green and the blue signal, are the detector separation and the GR marker separation, both of which can be determined from the processing.

Figure 5 illustrates the cross correlation process on real data as measured by CMI in SDM-1. The top figure shows the signals measured by the four detectors in the tool, where the depth of the first detector is depth-matched to the well. The plot in the middle shows the signals resulting from a cross correlation between the response from detector 1 and 2 (blue) and detector 1 and 4 (red). Both show three peaks. The highest intensity (most correlation) occurs when the signals are shifted by the separation of the two detectors, at which distance the signals from both marker 1 and marker 2 would overlap. Two satellite peaks of relatively high correlations occur for distances where the signal from marker 1 in detector 1 is overlapping with marker 2 in detector 2 and marker 2 from detector 1 is overlapping with marker 1 in detector 2. Knowing this, we can read off the detector separation from the location of the highest correlation, and infer the marker separation from the distance to the two satellite peaks. The bottom figure shows this process, where it has zoomed in on the three peaks of the cross correlation between detector 1 and detector 2. Note that besides the cross correlation no filters or alterations have been applied, the resulting signal is very smooth as all random noise features will cancel out in the process, leaving only clear peaks. The red lines in the plots are that of a Gaussian fitted to the peaks in the cross correlation.

Because there are four detectors on a CMI and FSMT tool, there are six detector pairs that can be cross correlated, resulting in six marker separation determinations per logging run.

The new cross correlation uses less input than the fitting method, in that it does not require knowledge of the detector separation. Instead, is generates the detector separation as an output, which can be used as a QC of the data processing. If, for example, there is some tool motion in between one detector passing a marker and the next detector passing, the tool might appear to be longer or shorter. Comparing the processed detector separation with those measured on site, one can detect unreliable data and remove from the interpretation.

Note that such movements are not detected by the fit method directly. There, the detector separation is a requirement for the analysis, so if there is some unknown tool movement, the measured marker peaks might be either closer or further apart than they actually are (the tool appears to be longer or shorter), and conversion with the (wrong) detector separation will result in an either too small or too large marker separation, which can only be picked up by seeing these results as outliers to separations determined from other runs or detectors.

Additional to the QC step of looking at the detector separation output, one can also look at the asymmetry of the signal. If all goes well, the satellite peak to the left of the detector separation peak in the cross correlation should be equal distance from the satellite peak to the right. If, again due to unexpected tool motion, the separation between two marker peaks in one detector's signal is

different from the separation recorded by the other detector, the signal in the cross correlation will be asymmetrical, and can be disregarded from final results.

We can see the QC steps in the example in Figure 5. It gives the separation between detector 1 and detector 2 of 1.5375m, whereas the field print mentions a separation of 1.5342m, a difference of about 3mm. The marker separations can be determined as 11.5242-1.5375=9.9876m, or 8.4547+1.537=9.9917m, being about 4mm different. In this case, this means that something has happened on a length scale of 3-4mm to the tool motion, and data should be marked as less reliable. If we refer back to Figure 1 and realise the two peaks we are looking at here are separated by almost 10m, a tool movement of 3-4mm is still very small and within the point spacing, but we are able to pick this up with the cross correlation method.

An example of a QC for a full data set is plotted in Figure 6, which is for FSMT data from 1982 in SDM-1. One thing that jumps out of these plots is the sudden decrease of the confidence level in both detector separation and asymmetry for marker pairs around 21-25 (these correspond to the depth interval ~3015mAHORT to 3034mAHORT). When we look at the log data, the measured cable tension is seen to change slightly across this interval, being the transition from gas/air in the borehole to water, which slows the tool down slightly. This signature in the QC plots is visible in all wells and different years, and does move up and down with the wellbore fluid level, and highlights the quality of these values as a QC step.

Besides aiding the analysis of the noisy data, the resulting peak shapes in the cross correlation will be more normally distributed from the random noise. In fitting methods, peak shapes are assumed to have a certain profile, most often Gaussian or Lorentzian, which in most cases will not affect the fitting of the central position of a peak too much, however for slightly asymmetric signals, the assumption of a symmetrical peak can cause certain bias.
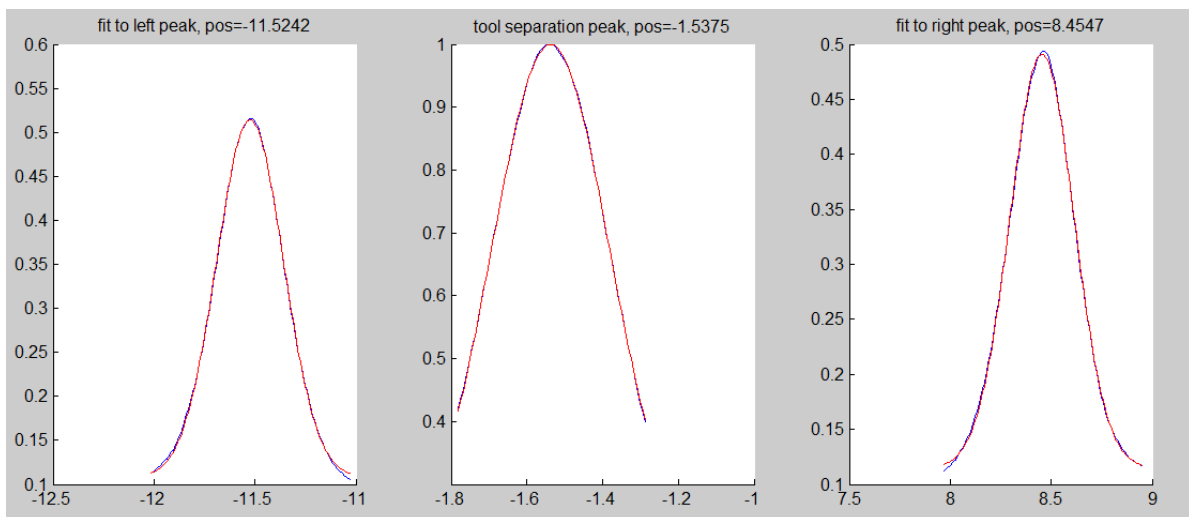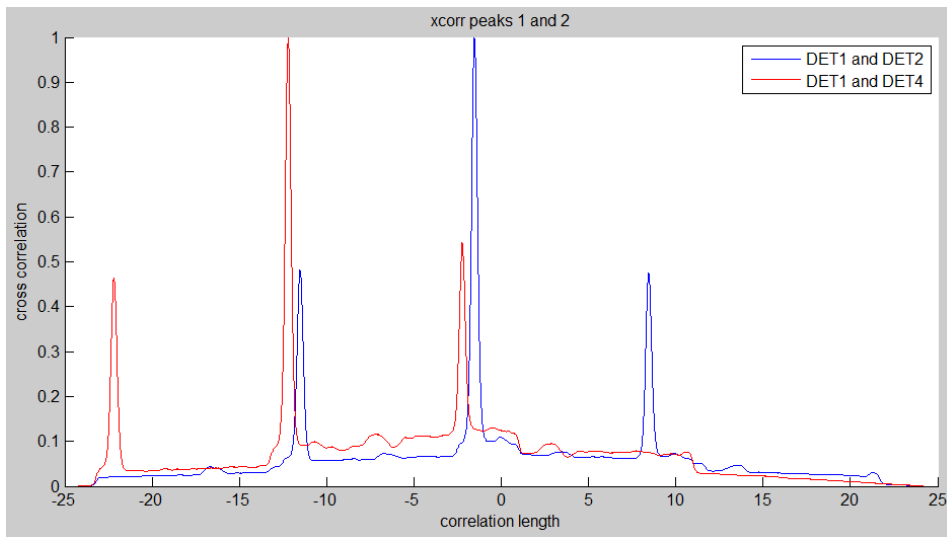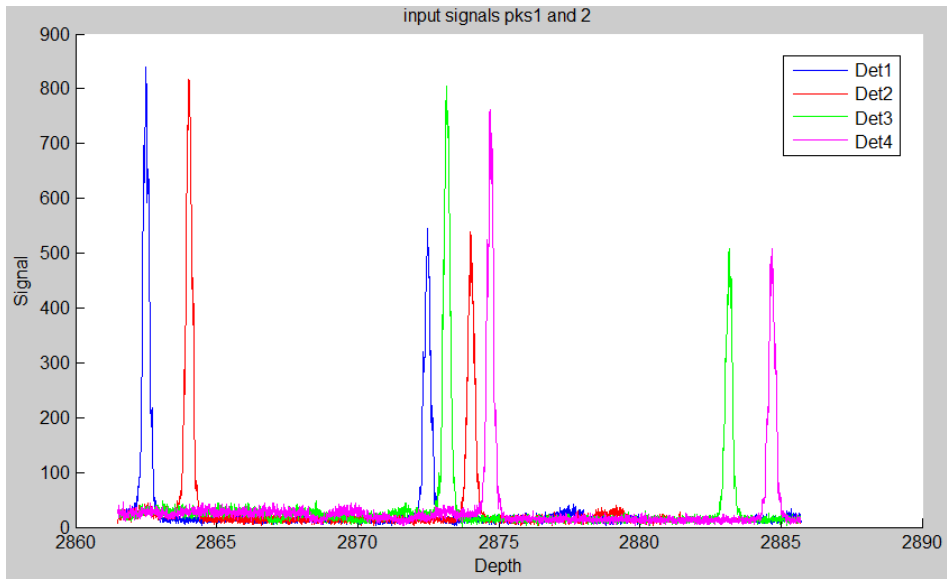
**Figure 5: Illustration of processing real CMI data using the new cross correlation method. Top figure shows the signals of two GR markers as measured by four detectors in the CMI tool. The second figure shows the resulting cross correlations from correlating the measured signals of detector 1 with detector 2 (in blue) and cross correlating detector 1 with detector 4. The bottom figure has zoomed in on the three peaks visible in the cross correlation between detectors 1 and 2. The blue is the resulting signal after cross correlating, the red lines on top are Gaussian peaks fitted to the signal.**
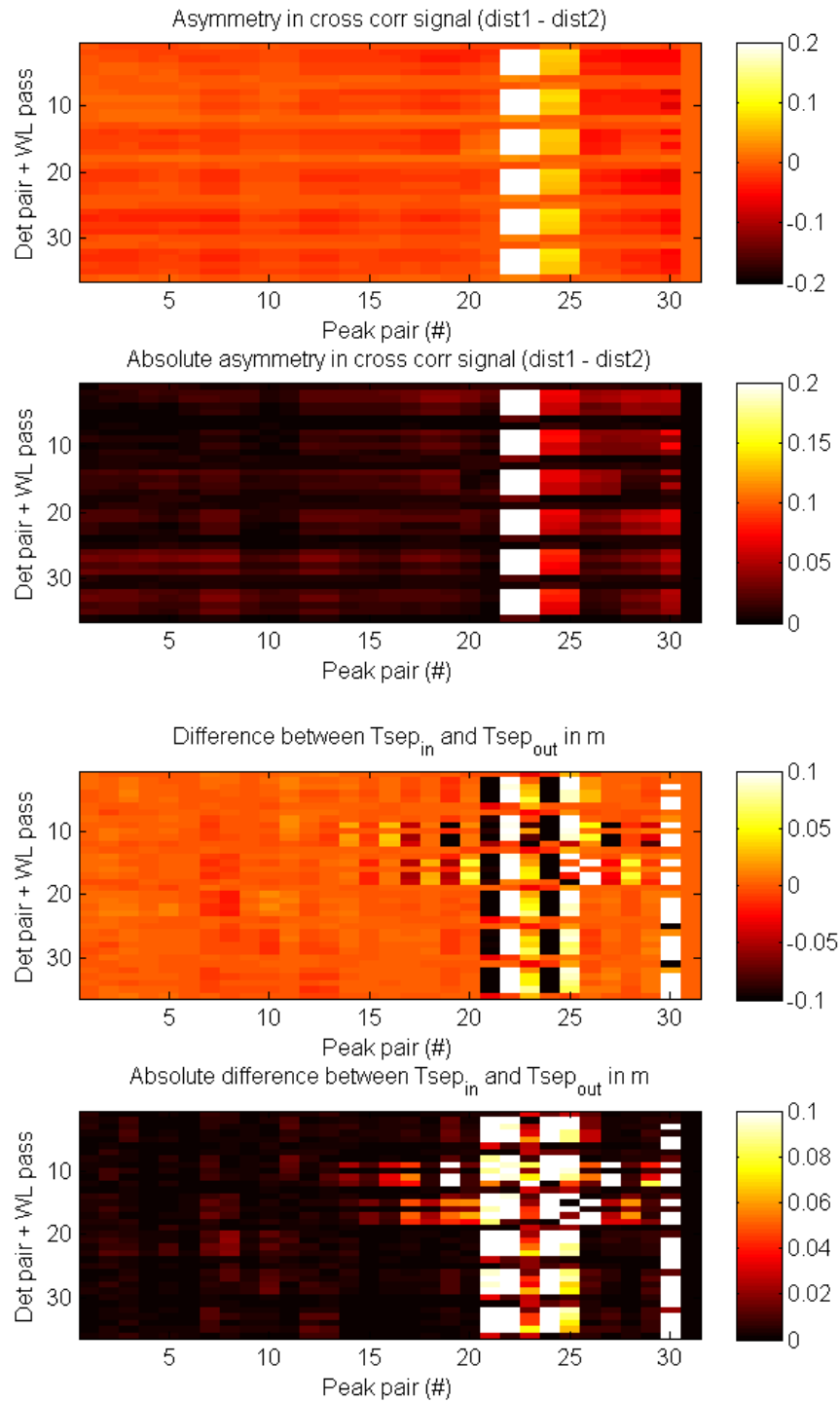
**Figure 6: QC plots for data from an FSMT run in 1982 in SDM-1. Top plots compare the asymmetry in the cross correlation signal, bottom plots compare the output detector separation with the measured separation. On the y-axis, the results are plotted as a function of the detector pairs (6 per run) and number of runs. In this case, there were 6 wireline runs, resulting in a total of 36 separation determinations. On the x-axis, the marker pairs are plotted.**

# 4 Simulation and testing

To test and demonstrate the accuracies of the different analysis methods, we generate signals similar to those measured, where in the simulation we know the marker separation. The outputs of the different methods can then be compared to the known input.

First, we describe the theoretical shape of the measured signals, to determine if a Gaussian or Lorentzian fit should be preferred, and to check that the widths of these peaks as measured by FSMT and CMI are as expected, with little experimental broadening. The theoretical description is followed by some characteristics seen in the data, like noise levels and count rates, so we can make the simulated signals as close to those seen in the field. Then, we apply the analysis routines to the simulated signals to determine their accuracy. From the known time-decay of the gamma ray intensity with the $^{137}$Cs half-life, we use these simulations as well to predict when certain markers can still be used reliably in the in-situ compaction measurements.

## 4.1 Theoretical line shapes of radiated intensity

The intensity as radiated by the marker decays both from a geometrical factor (expansion of the spherical emission through space) and from an absorption by surrounding matter. The geometrical decay as a function of distance to source $r$, scales with the inverse area of a sphere: $I_{geom} = \dfrac{I_0}{4\pi r^2}$ .

The decay through absorption depends on the absorption capacity of the material around the marker. Assuming the casing and mud in the well bore can be neglected compared to the absorption by the formation (compared to the formation, both the mud, casing and cement are of much more constant absolute thickness as a function of observation angle, and can therefore to a first approximation assumed to attenuate the signal more homogeneously when passing a GR marker), the decay through absorption is: $I_{abs} = I_0 e^{\frac{-r}{r_0}}$ , where $r_0$ is the rate of absorption of the formation, $r_0 = 1/(\rho\mu)$ where $\rho$ is the bulk density and $\mu$ the mass absorption coefficient. For sandstone, the mean mass absorption coefficient for $^{137}$Cs gamma ray radiation is 0.0761 cm$^2$/g [7], and with a bulk density of 2.30g/cm$^3$ (peak in measured density histogram for SDM-1 well data), $1/r_0$ = 0.175cm$^{-1}$, or $r_0$ = 5.7cm. This value means that the gamma ray intensity is halved approximately every ln(2)*6cm = 4cm in sandstone.

The observed intensity, at a distance $r$ away from the source, then becomes:

$$I = \frac{I_0 e^{\frac{-r}{r_0}}}{4\pi r^2}$$

In terms of the intensity measured at a location $x$ along the borehole, with a marker at depth $x_0$ and placed at a depth $d$ into the formation, $r^2 = (x - x_0)^2 + d^2$. Note that the shape of $I(x)$ is more Gaussian if the absorption term is more dominant (deeply buried markers), and more Lorentzian if the geometric term is more dominant (shallow markers, $d$ small compared to $r_0$). Here, we stick to using a Gaussian fit for now as for fitting the peak position, the difference is expected to be minimal.

Simulated line shapes for a range of *d/r₀* values are plotted in
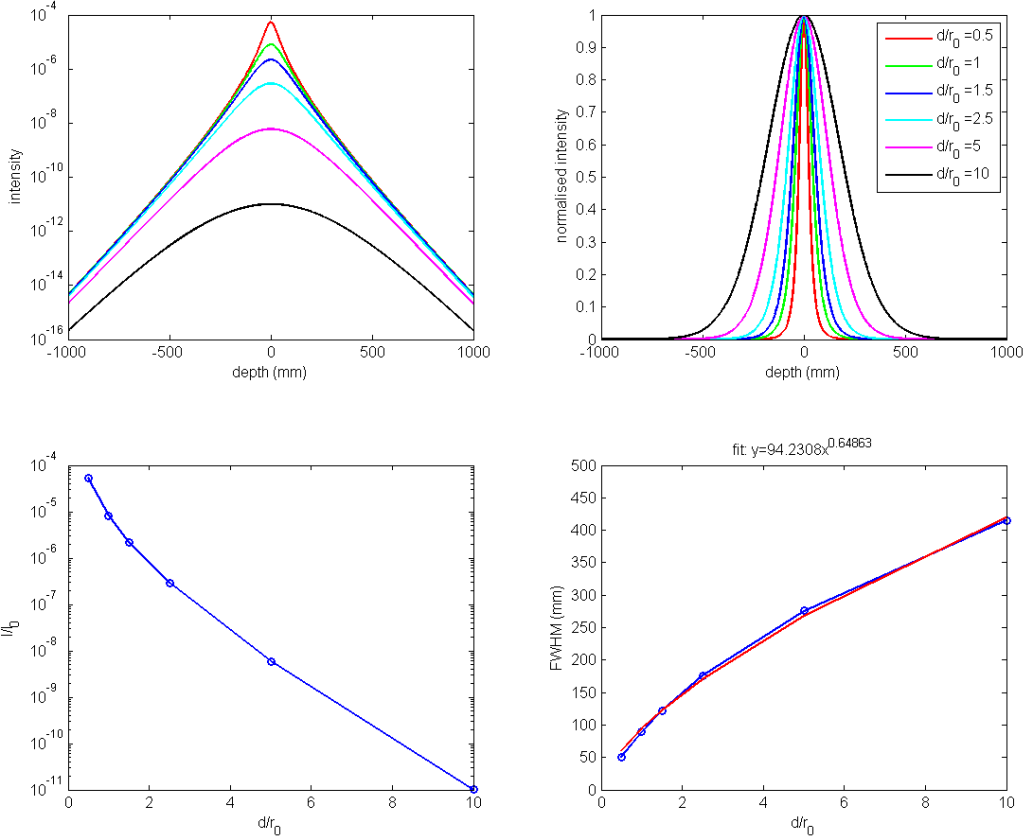


Figure **7** including their intensity reduction and FWHM. It shows that for all marker depths *d*>60mm, the FWHM is expected to be more than 100mm, i.e. the measured peaks expected are inherently much wider than the expected compaction on the order of mm's, and this cannot be improved by different tool design.
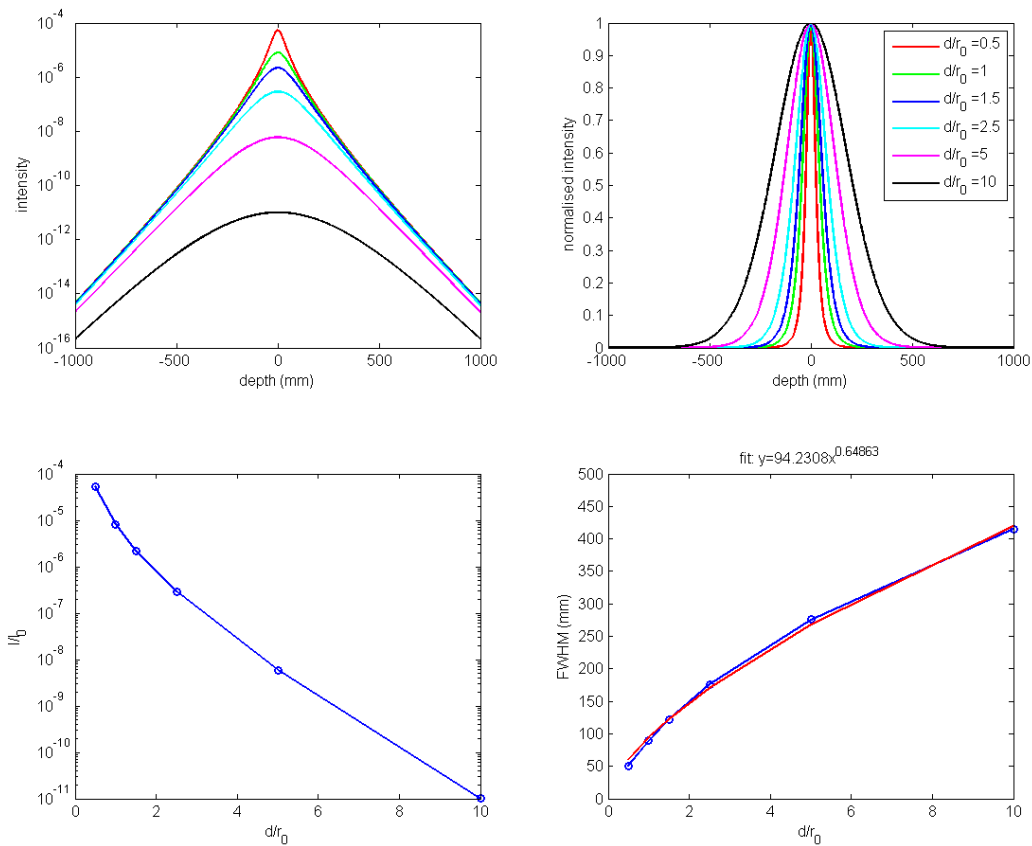
**Figure 7: Simulated line shapes, with corresponding intensity and FWHM dependency on *d/r₀* (ratio between marker depth and gamma ray absorption). A fit of the form a*x^b to the FWHM as a function of *d/r₀* gives FWHM = 94*(*d/r₀*)^0.66, where *r₀*=60mm.**

From the SDM-1 data, we see by fitting a Gaussian to the peaks and converting their widths to d/r0, we get a range of approximately 4 < d/r0 < 7, or 240mm < d < 420mm as an approximate range for burial depth of the GR markers. Resulting ranges in intensity from the theoretical line shapes are a factor of 60 between shallowest and deepest buried markers, in line with a spread of roughly a factor of 40 in the measured data by CMI (ignoring the age of the markers).

## 4.2   Additional problems in the real signals

Tool movement other than vibrations (vibrations will add a noise like component), like stick-slip. These can be detected in the cross correlation method from the asymmetry and tool separation outputs. See for example SDM-1 and ROT-1 results, where stick-slip signatures are detected in the analysis, which occur at a location in the well where cable tensions do not behave normally.

Temperature effects: the expansion coefficient of different steel types is roughly 10e-6 – 15e-6 m/m/K. As the tool length is in the order of 10m (the detector spacing), a 10degree temperature difference creates a length change between the detectors on the order of 1mm. Throughout the

reservoir section, the temperature changes by about 5-6 degrees C as recorded by the tools, which would result in a change on the order of 0.5mm in detector separation. Besides changes in the tool dimensions, the length of the wireline cable will be thermally altered.

Optimal separation: The compaction tools (both FSMT and CMI) benefit from detector separation being more or less identical to the bullet separation. In real life, however, the separation between the bullets is generally different from the optimal detector spacing, reducing the effectiveness of the analysis method. The difference between the detector and bullet spacings can be seen in Figure 5, where the intensity from neighbouring as measured by different detectors do generally not overlap.

The intensity of the peaks will decay with time, due to the radioactive decay of the $^{137}$Cs markers. The half-life of $^{137}$Cs is about 30years, which gives a decaying signal intensity over time as illustrated in Figure 9. Due to the decay, peaks that are still clearly visible above the noise now, might not be detectable with accuracy in the future. In the simulation, we will therefore look at the accuracy of the separation determination as a function of signal intensity to investigate the expiry date of certain marker pairs.
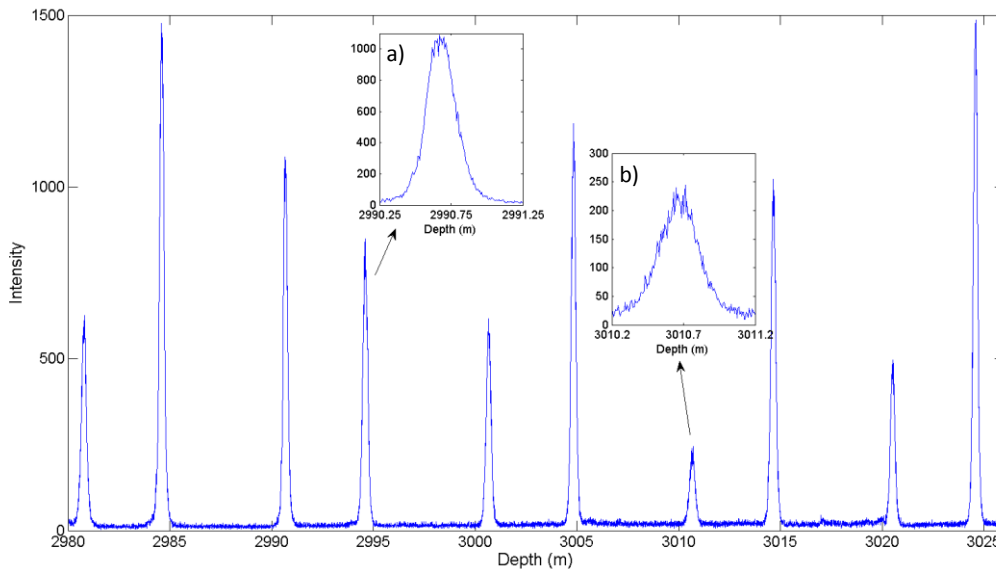


**Figure 8: Measured gamma ray signal in Stedum-1 in 2010 survey, as recorded by Detector-1. A typical section of the signal along the well is shown, with insets of two peaks; one with a peak intensity around 1100 counts in (a), close to that of the average intensity, and one with a very low signal in (b), of about 250 counts. The intensity of peak (b) is the what is expected for an average peak intensity around 2070. Note that the widths of the insets are 1m, showing the broad nature of the measured peaks.**
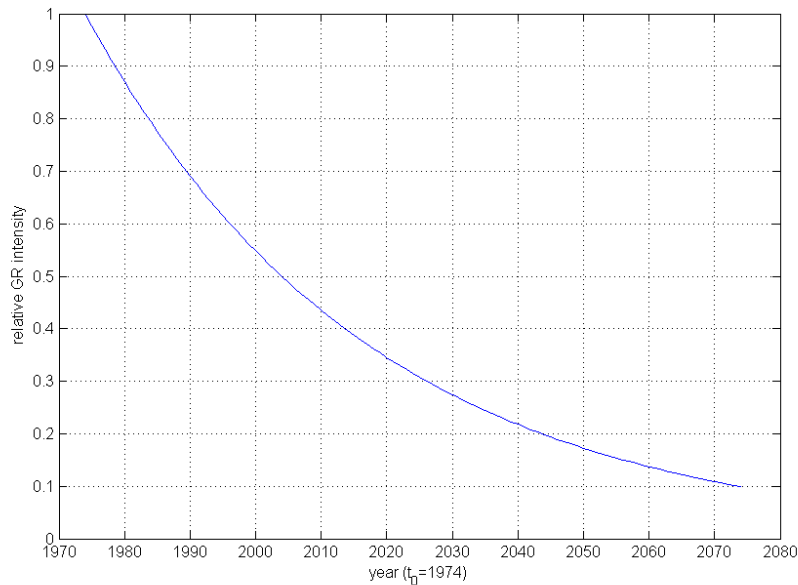
**Figure 9: Intensity decay for Cs-137, with half-life of 30 years. Set t=0 to 1974, when markers were installed?**

## 4.3   Typical GR signal characteristics

The signals as measured by the gamma ray detectors are a convolution of the emission profile, detection function and unknown/unexpected tool motion.

The shape can be approximated by a Gaussian or Lorentzian peak. For determining peak position, however, the difference between a Gaussian or Lorentzian should not matter too much. The peaks have a certain width, depending on both tool response and how deep the GR marker has penetrated into the formation (according to 1997 report, this is roughly between 20-70cm [3]). The shallower the burial, the wider is the signal. To estimate the range of widths of these peaks, we fitted Gaussian (or maybe Lorentzian) peaks to all the measured data in Stedum in 2010 and 2013, resulting in an average FWHM (full width at half maximum) of 0.27m, minimum FWHM of 0.20m and maximum FWHM of 0.34m. Note that these peaks are much wider than the level of compaction that we are trying to measure, which is only several millimetres between surveys.

The noise on the measured signal is a combination of the (shot noise) emission of the gamma ray sources, the noise in the signal detection, and also the vibrational noise in the position of the tool. From the Stedum data, we see noise levels between 1 and 4 times normal shotnoise, with an average of about 2.5 (using the definition noiselevel = observed spread in intensity / sqrt[average intensity]. In this definition, pure shot noise is expected to have noiselevel around 1).

The peak maximum intensity from the Stedum data ranges from about 100counts to 4300counts, with an average peak height of 1200counts. Each of the four detectors in the tool have a slightly different level of detection, with a maximum difference of roughly +/- 3% in measured intensity levels. As the gamma ray sources will decay over time, the intensity levels are expected to decrease with time. The half-life of Cs-137 is about 30 years, so the average intensity levels (as measured by a CMI tool) will drop to around 600counts around 2040, and 300counts in 2070. See Figure 9 for

theoretical emitted intensity relative to time of marker installation in 1972. We will address the drop in intensity with time in more detail later on when we discuss the dependence of the measurement accuracy with signal parameters.

The gamma ray signal is sampled (at least by the CMI tool) on 5-6mm intervals.

## 4.4 Simulated signals

To test the interpretation accuracy of the different methods, we generate typical signals (Gaussian peaks) with a known distance between the gamma ray bullets. As both the FSMT and CMI tools have four detectors, we generate four signals offset by the detector spacing. We use the following:

```
y1=Det1amp*(A1*exp(-(x1-P1).^2/w1^2/2) + A2*exp(-(x1-P2).^2/w2^2/2))+bgrnd;
y2=Det2amp*(A1*exp(-(x2-P1).^2/w1^2/2) + A2*exp(-(x2-P2).^2/w2^2/2))+bgrnd;
y3=Det3amp*(A1*exp(-(x3-P1).^2/w1^2/2) + A2*exp(-(x3-P2).^2/w2^2/2))+bgrnd;
y4=Det4amp*(A1*exp(-(x4-P1).^2/w1^2/2) + A2*exp(-(x4-P2).^2/w2^2/2))+bgrnd;
```

Here, y1, y2, y3 and y4 are the signals as measured by the detectors, each weighted by a relative detector efficiency (Det1amp, Det2amp, etc) to mimic the difference in measured countrates. Both generated peaks have an amplitude, A1 and A2, and a width, w1 and w2 (where FWHM = 2*sqrt(2*ln(2)) * w)
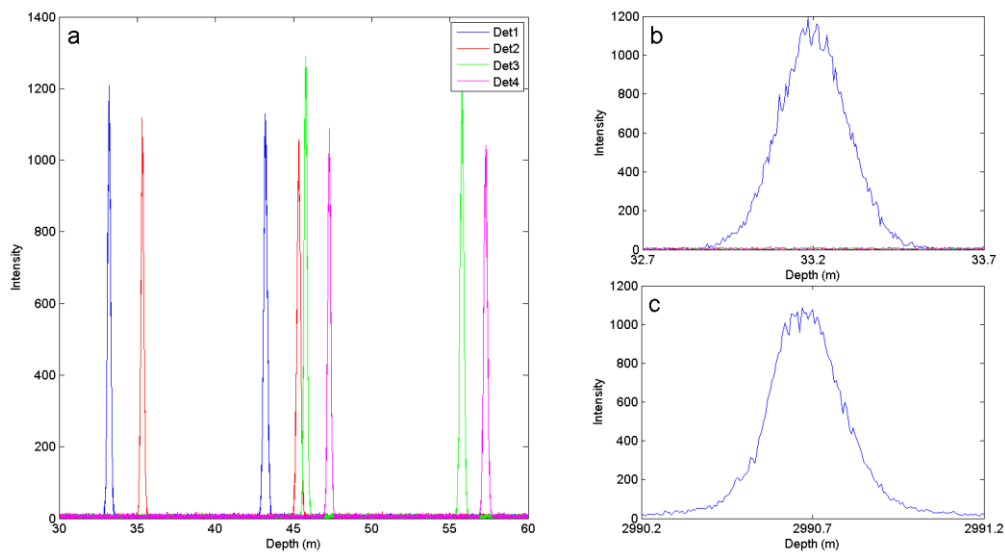


**Figure 10: Generated signal, in a) for all four detectors, and in b) zoomed in on one of the peaks. Panel c) displays a real peak from the SDM-1 2010 data, showing the similarity between the generated signals and the actual signals. Difference in the tail actually suggests that a Lorentzian function might better describe the measured peak shape (Gaussian decays to zero faster than a Lorentzian).**
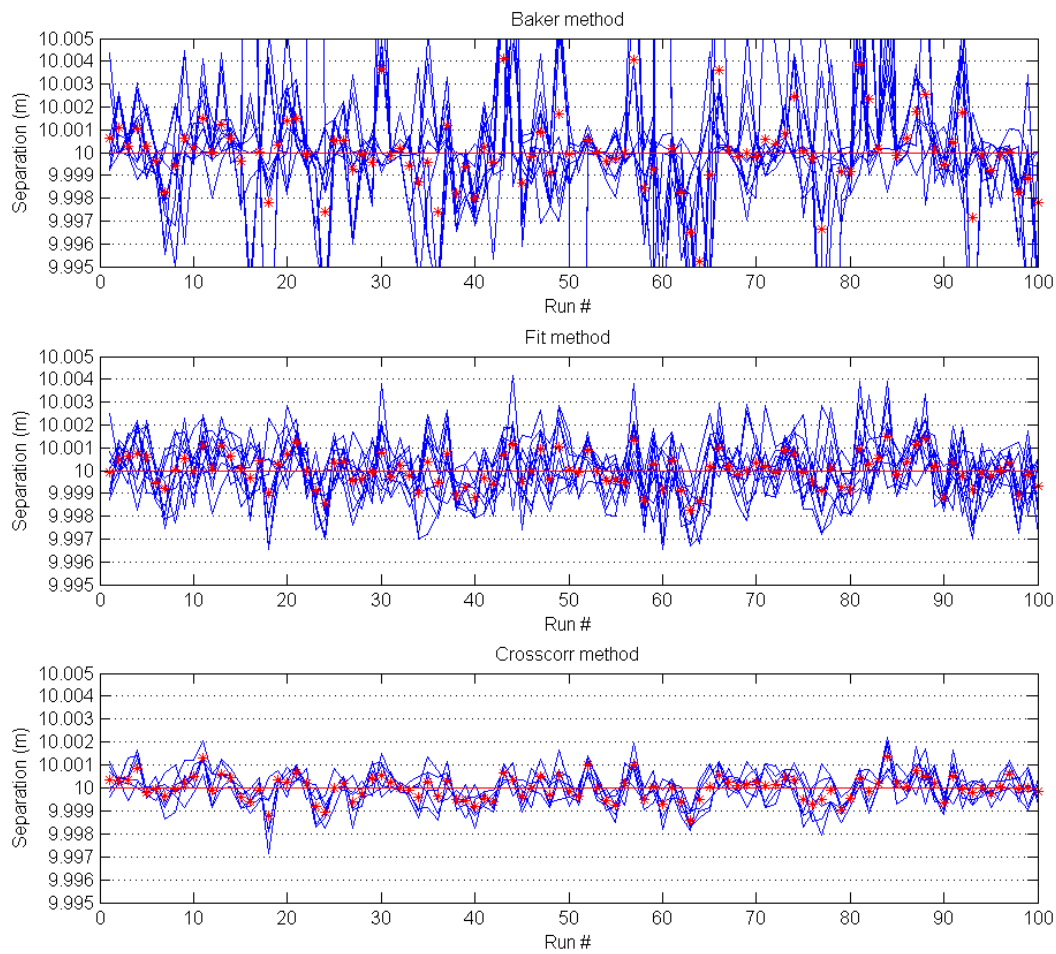
**Figure 11: Interpreted GR bullet separation for 100 simulated signals, using the three different interpretation methods. Signals had random noise (using fnoise = 2.0), fixed widths but random amplitudes, around 1100 counts. The blue lines show the interpreted separations from the different detector pairs, the red dots show the average separation from these detector pair results. The red line shows the input separation of 10m.**

The deviations in the simulations above represent sort of the intrinsic error in the measurement interpretation, as 'perfect data' is used, where perfect refers to the fact no unnoticed tool movements are simulated.

The deviations from the input show that generally the uncertainty in the analysis is larger than 1mm, which has been noted by other studies [2], [8], whereas the 1mm is only approached by the cross correlation method introduced here, and only for data without unexpected tool movement.
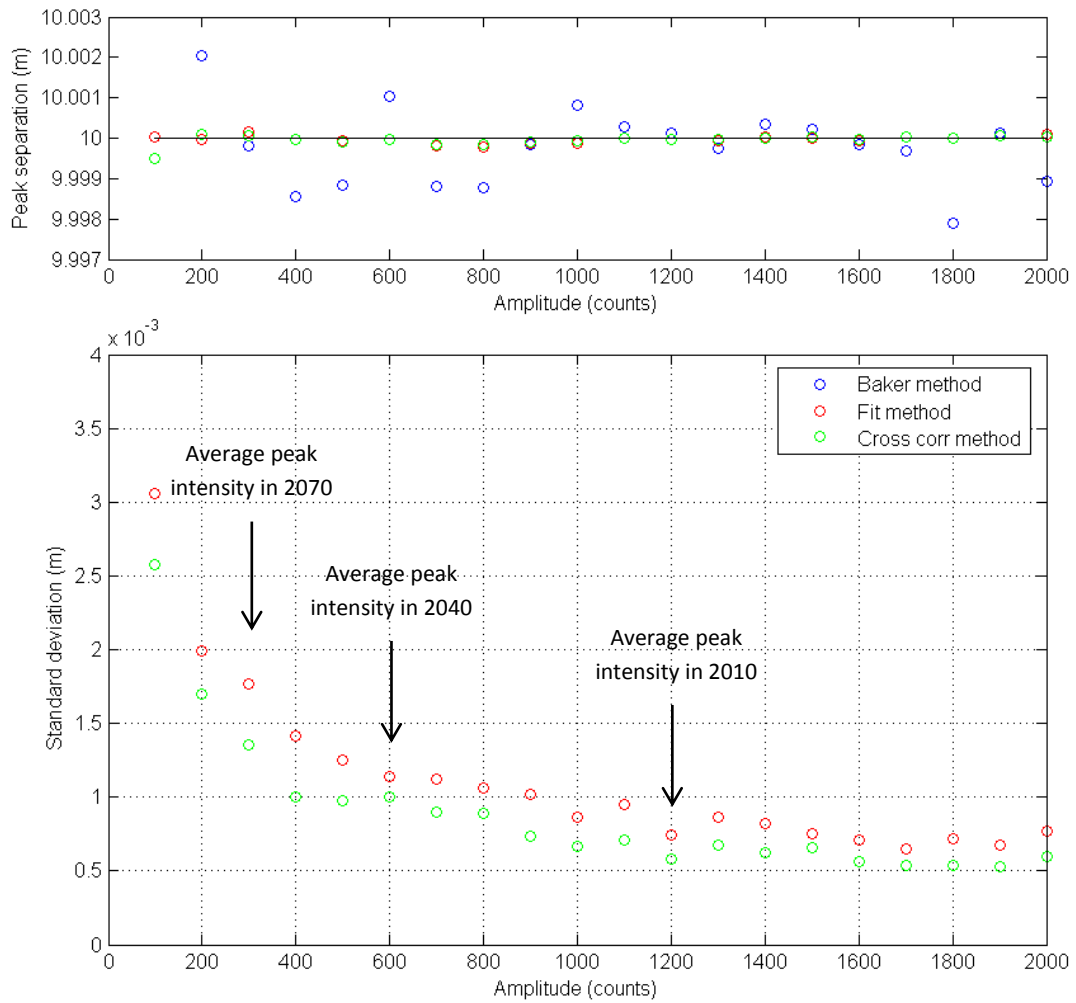
**Figure 12: Output results from the three different methods as a function of average peak amplitudes of the generated signals. The generated peaks had a FWHM of 0.3 and were separated by 10m. A random noise with a standard deviation of 2.5\*sqrt(intensity) was added to the signal, to resemble field data. For each data point in the figure, a total of 100 signals were generated and evaluated. The average peak separation is shown in the top panel, the standard deviation over these 100 samples is plotted in the bottom panel. The standard deviation resulting from the Baker method was always >5mm so does not fit on the figure's scale.**

# 5 Data availability

To re-analyse the historic data, the raw intensity data needs to be available. For some of the wells, only filtered and/or interpreted data existed digitally. Missing data has been sourced through the logging companies, and some retrieved from archived tapes (Exabyte and 9Track), however not all data from all historic FSMT / CMI runs has been retrieved. Tables of available digital and print data have been included in the appendix of this report for all the wells in the Netherlands which have GR markers installed.

The most complete raw data sets are available for Stedum-1 (SDM-1). We first focus on the SDM-1 data to test the method, before applying the new analysis technique to all other wells. The SDM-1 well has the additional benefit that several test runs of different tool string setups was done for the Baker CMI tool in 1997.

# 6 Analysis of Stedum-1 compaction

We first apply the new analysis method to the well where most survey data is available, which is Stedum-1. See the tables in the Appendix for surveys of which the raw data is digitally available, which can be analysed using the new method. We go through the data year by year, and compile the results afterwards.

**FSMT data, 1982**

*March* - The FSMT tool was first deployed in 1982, and was tested along with the PDM tool it was replacing in March, April and September. In the March data (three runs), some of the detectors failed occasionally giving no counts for a significant part of the well. Additionally, the data shows severe stick-slip or similar issues resulting in very blocky peak shapes, see Figure 13. Hence, we do not analyse the March data further.
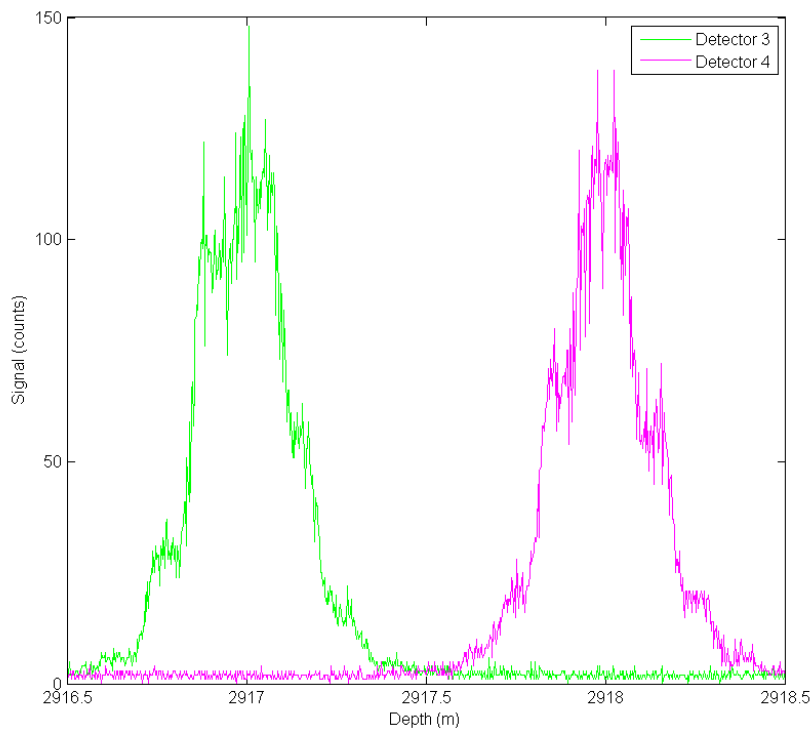


**Figure 13: Peaks measured in the March 1982 survey by FSMT tool. Blocky nature of the peaks suggests severe stick-slip, with intervals of regularly more than 10cm, making data analysis unreliable for compaction studies. Moreover, Detector 1 regularly did not register any counts (zero over the interval in this figure) and Detector 2 recorded with much higher background than the other detectors.**

*April* - In April, another survey of both FSMT and PDM were performed. No detector spacing measurements are known (not mentioned on the prints). We therefore perform a cross correlation of the full intervals, and use the maximum in those spectra as a measure for the detector spacings. As the current analysis method does not require an accurate spacing as input since it only uses the spacing as a check for unexpected tool motion to remove unreliable data points, the estimated spacing does not affect the actual measured marker interval lengths. At most, it could result in intervals to be wrongly marked as either reliable or un-reliable, however these are expected to be rare as the asymmetry QC step is not affected by the detector spacing. Figure 14 below shows the marker intensities measured in April 1982 for the same GR markers as plotted in Figure 13 for March 1982. The blocky nature is reduced, although still present (see the left shoulder of the marker as measured by Detector 3), possibly by removing the centralizers from the tool string or making other changes to the logging operations (detailed tool string sketches not available on the prints). The cable velocity does show periodic fluctuations throughout the wellbore, at 5-10m intervals, with amplitudes of the order 0.05m/min (average logging velocity ~1.6m/min).
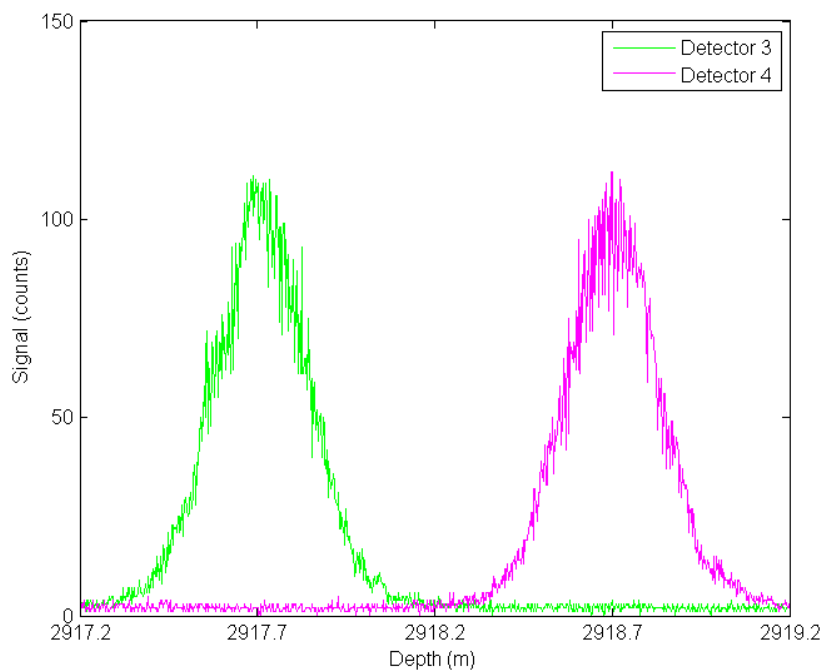


**Figure 14: Peaks as measured by FSMT tool in April 1982. Same peak as in March 1982 data in Figure 13, however now the blocky nature due to stick-slip has significantly been reduced compared to March 1982. Window width is the same for both figures (2m)**
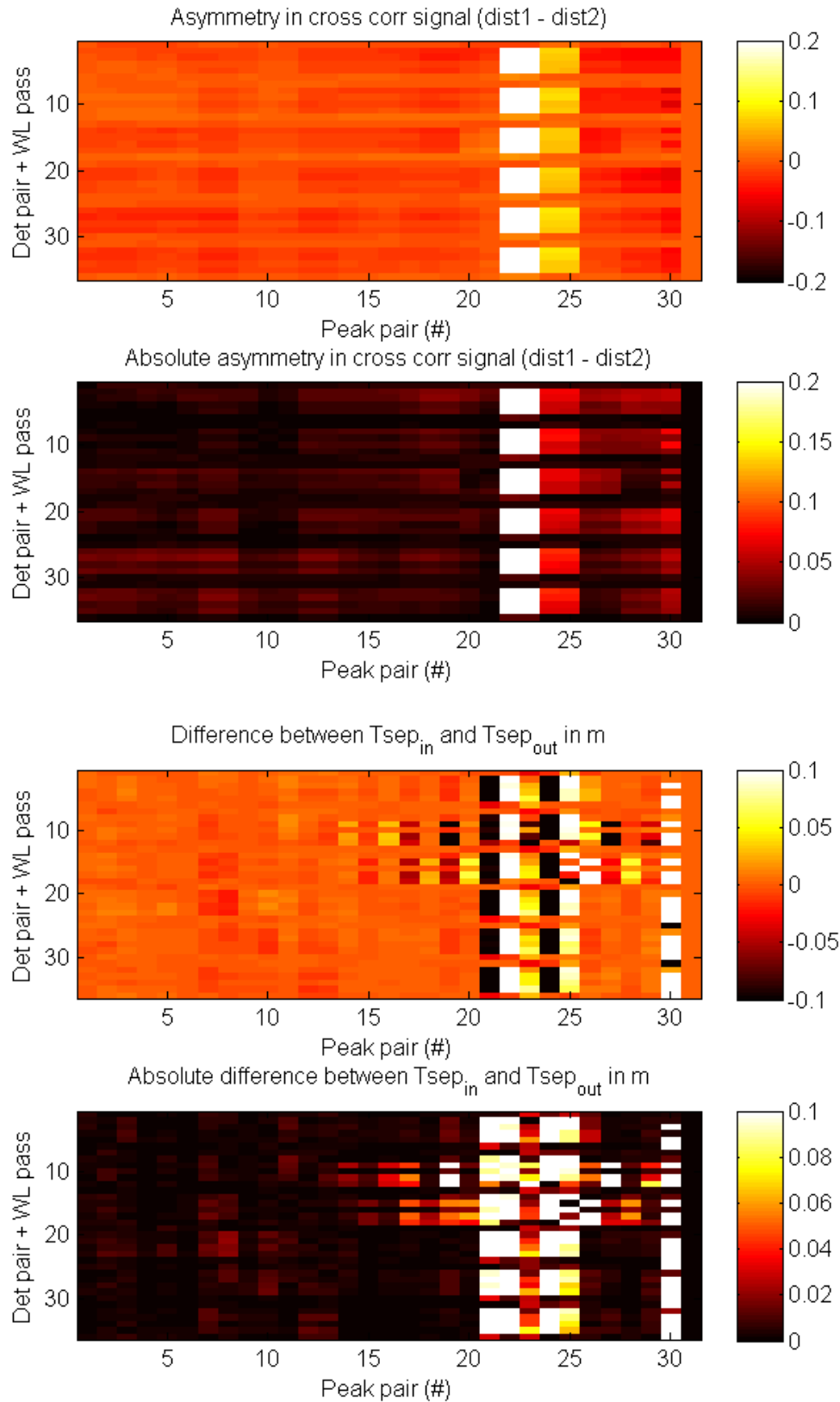
**Figure 15: QC of the 1982 data. Top: looking at the cross correlation asymmetry, bottom: difference between measured and determined detector separations. Vertical axis corresponds to detector pair and wireline pass (6 pairs per pass, 6 passes total), horizontal axis gives the peak pair, starting at the shallowest marker intervals. Clearly some issue around marker pairs 21-26, and around 30. Interval 21-25 corresponds to depths of 3015 - 3034 mAHORT, which coincides with a change in cable tension and liquid level in the borehole.**

**CMI, 1997**

A test was done of the new Baker CMI tool in SDM-1, comparing different tool centralisations. Three runs were performed with a centralized tool, 5 without any centralizers, and another 3 with the back-up tool and eccentric roller bars. A Baker report mentions that the results without centralizers or with roller bars are the best, as with the centralizers there is too much stick-slip. Here, we ran the analysis on all data and also found that the setup using standard centralizers gave the poorest results, having higher deviations in the output and generally higher asymmetry values.
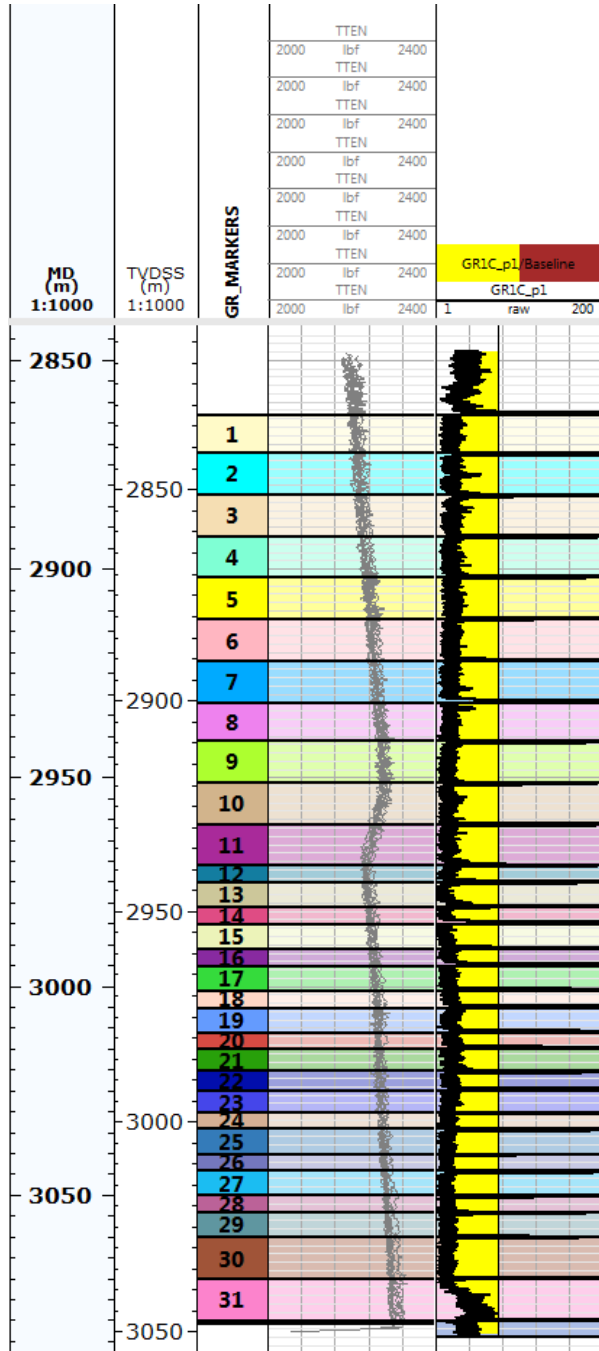


**Figure 16: Cable tensions for CMI runs in SDM-1 in 1997. Transition in tension observed round marker interals 10 and 11, due to the transition from gas to liquid in the borehole.**

## 6.1 Cable speed and tension

Below are some figures illustrating the cable speed and tensions as measured at surface and in the tool head, which can be used to see significant stick slip issues. Throughout time, tools have been improved such to make the logging smoother, as evidenced by the figures below.

You can see that certain runs have a wider spread in velocity and/or tension, resulting in less reliable results. Also strong oscillations in the cable speed in particularly the 1980s data. CMI data from 1997 shows that, in line with findings above from the cross correlation QC, that the cable tension is higher when using centralizers, even though the speed is lower. The spread in cable speed is also much wider than when not using centralizers, indicating that runs without centralizers and roller bars are better/more reliable data.

Note that only some issues can be detected in the speed and cable tension, very fine and small (mm-scale) events easily go unnoticed. Especially in the cable speed, which is measured at surface.

Cable velocity and tension, April 1982:
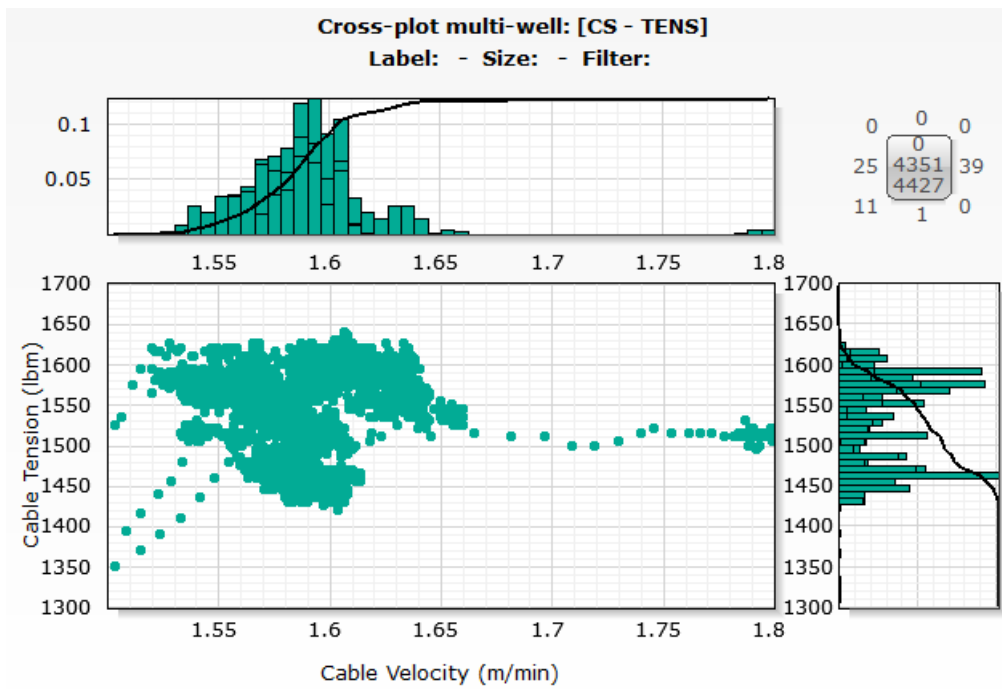


Cable velocity and tension, Sept 1982:
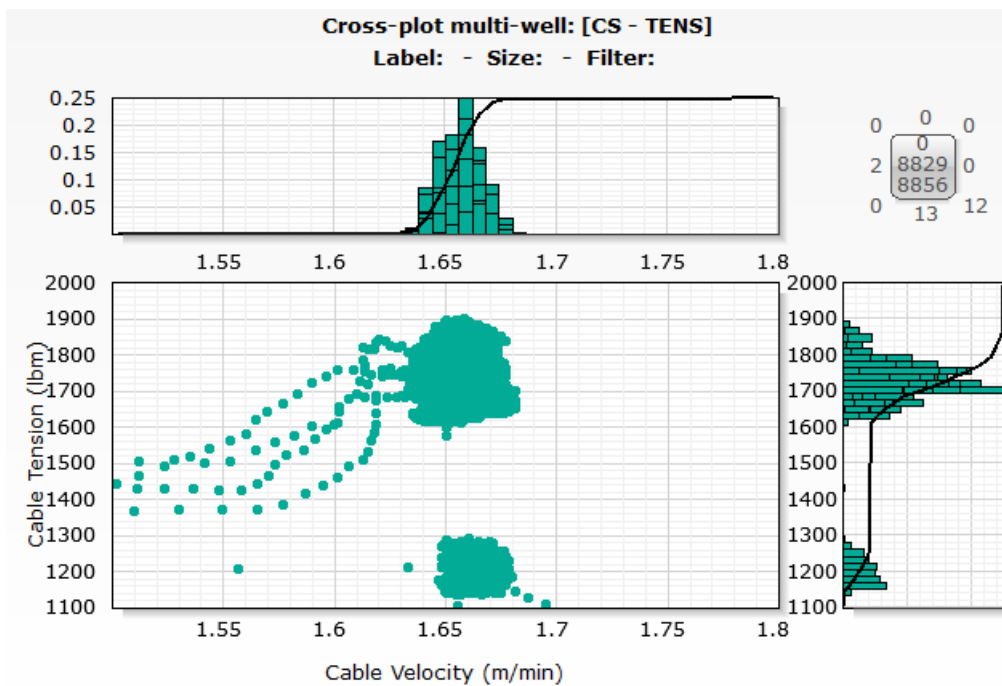
Cable velocity and tension, 1984:
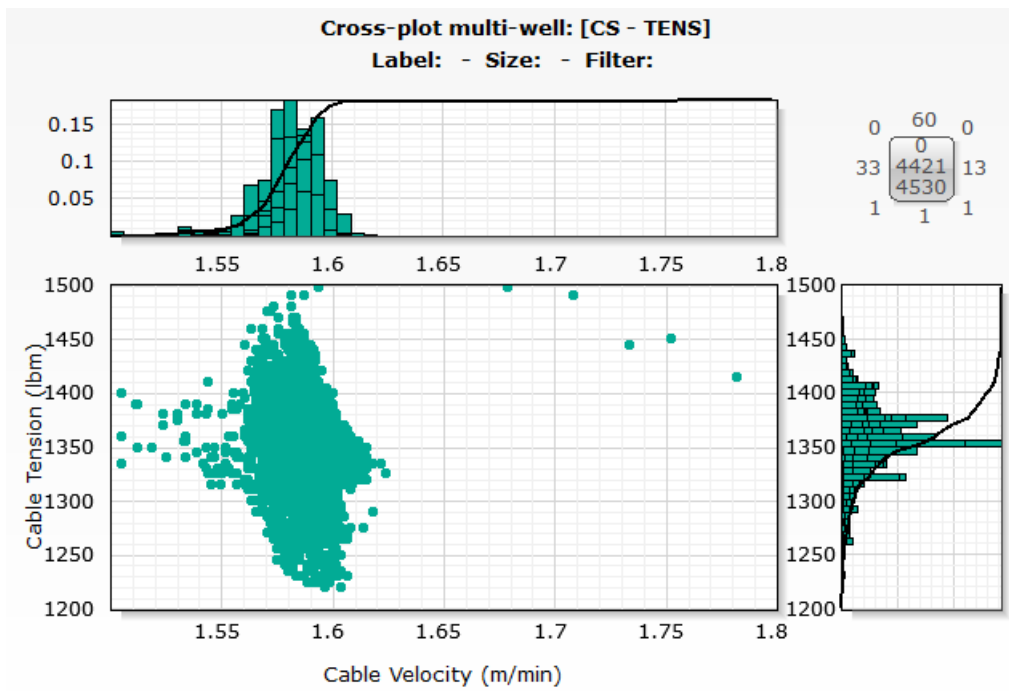


1986:
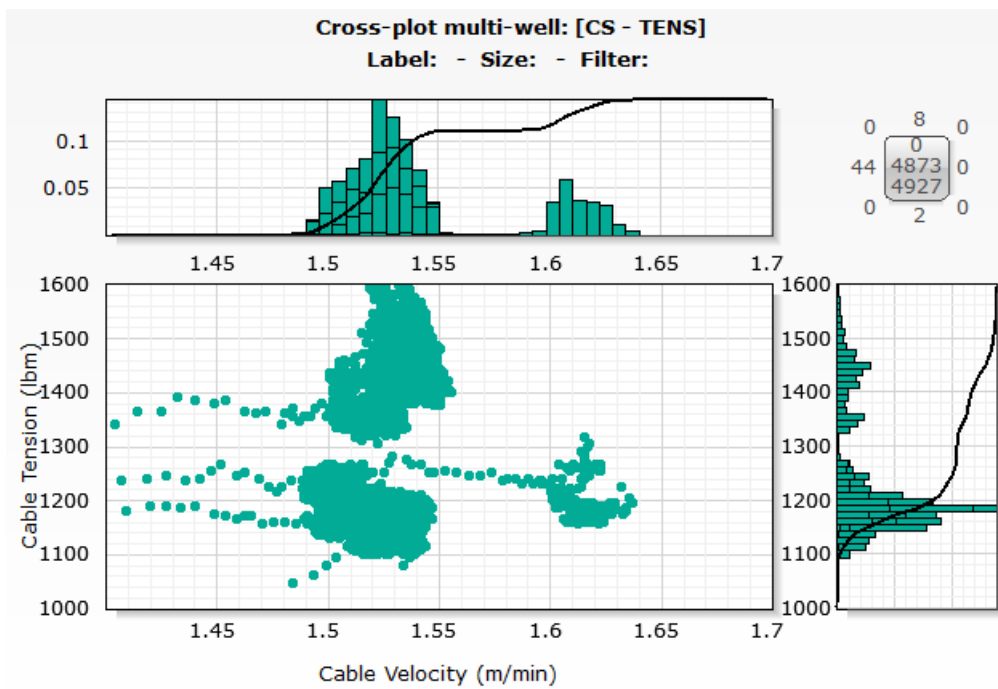
1997 CMI data, three different setups.

Blue: with centralizers

Red: without centralizers

Green: with rollerbars, no centralizers
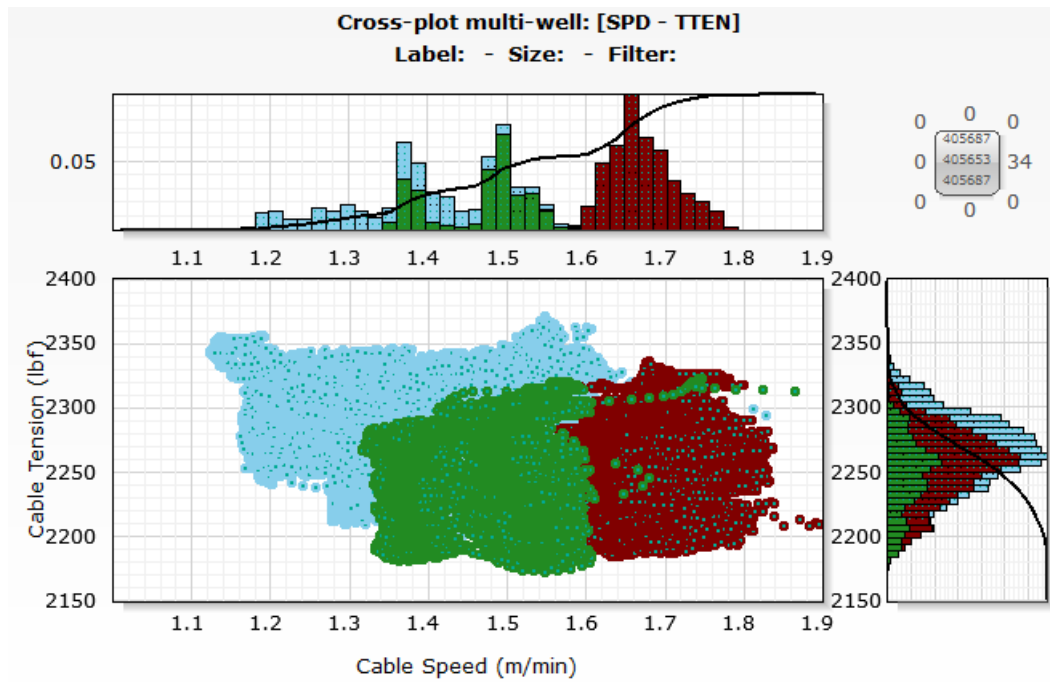


2005 FSMT:
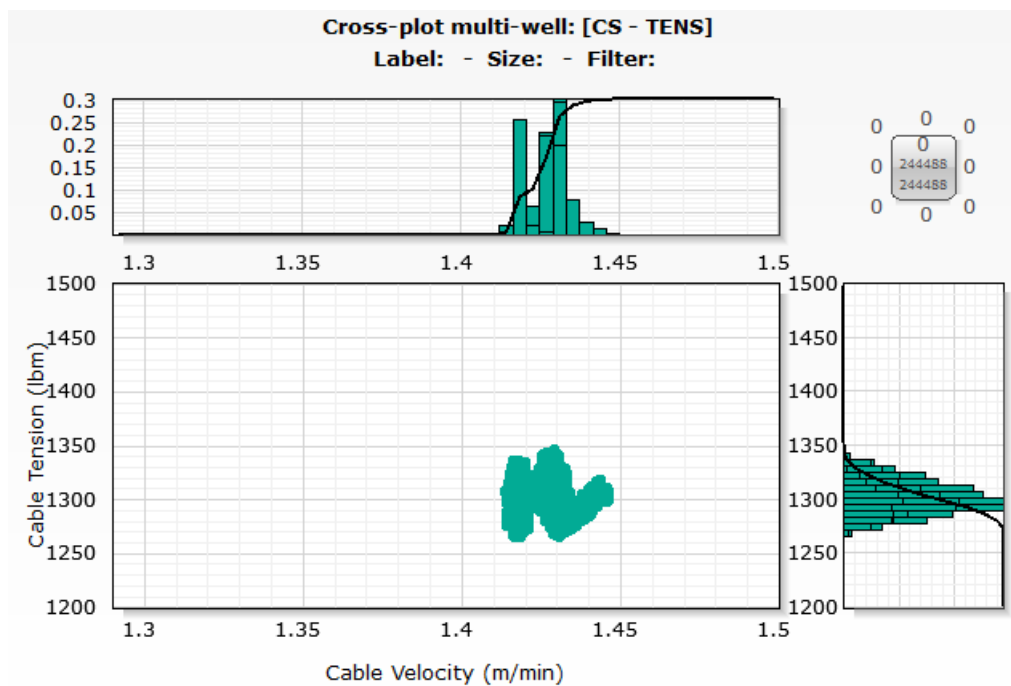
2010 CMI data:
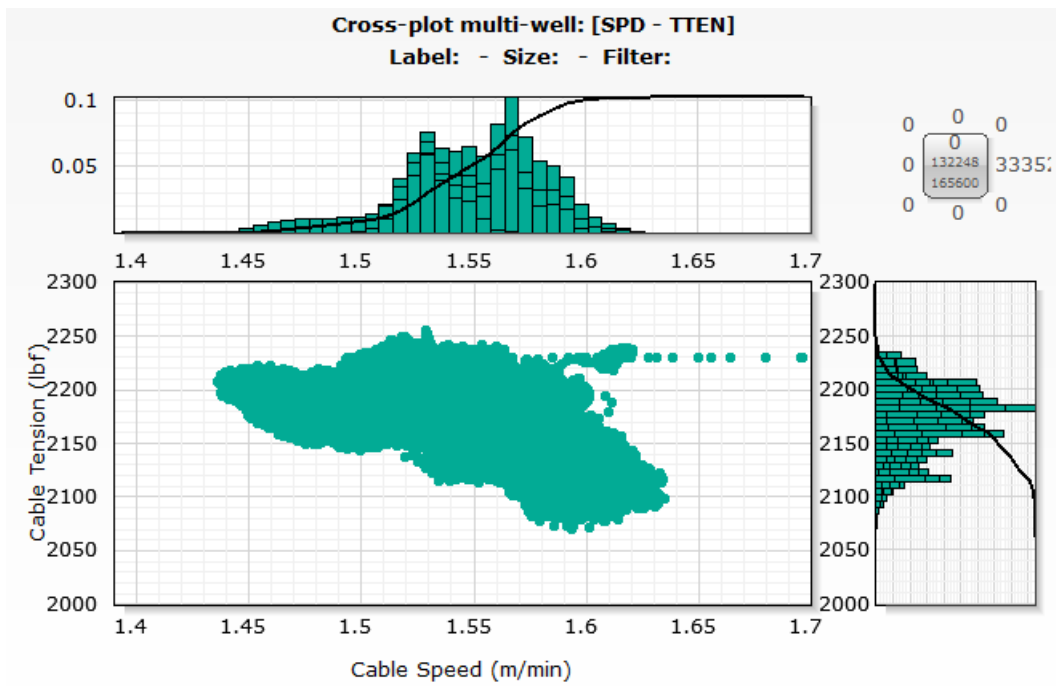


2013 CMI data:
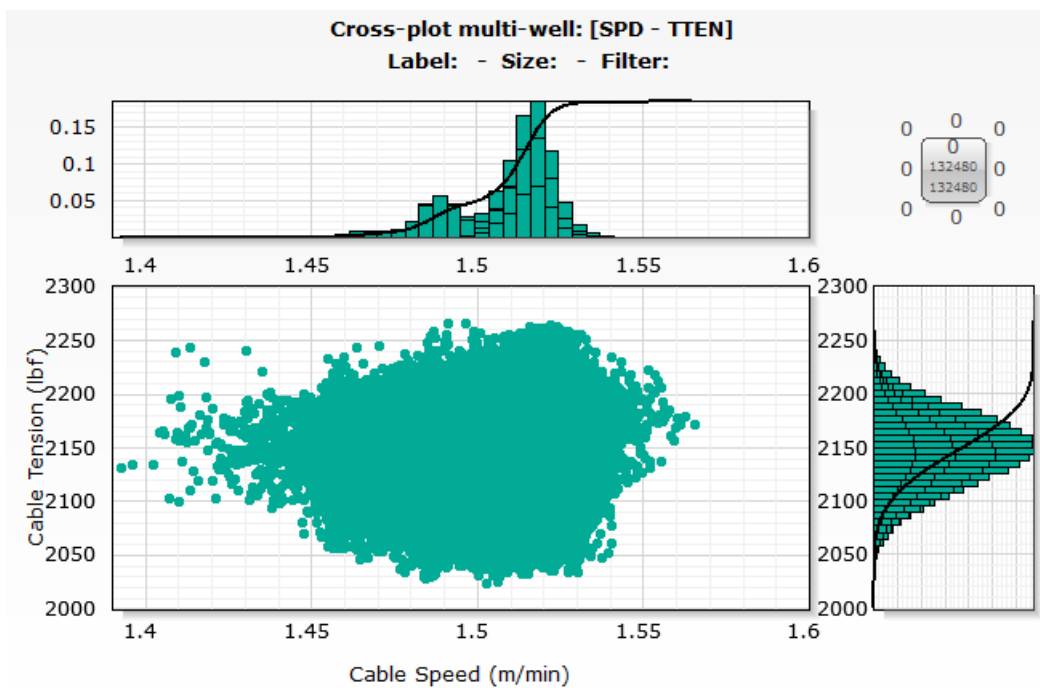
## 6.2 First pass results

A first processing pass has been performed on the data from SDM-1. Below are some figures showing the preliminary data resulting from the workflow. The workflow has to be refined further to optimise output. The QC and data rejection steps, for example, can be made more efficient. Now that the scripts are working and that data is processed such that it can be fed into the workflow, analysis can be done to determine best parameters and scripting optimisations.

Supporting data, such as average porosity and reservoir pressures per interval, are combined together with the compaction values in Techlog for correlation checks.
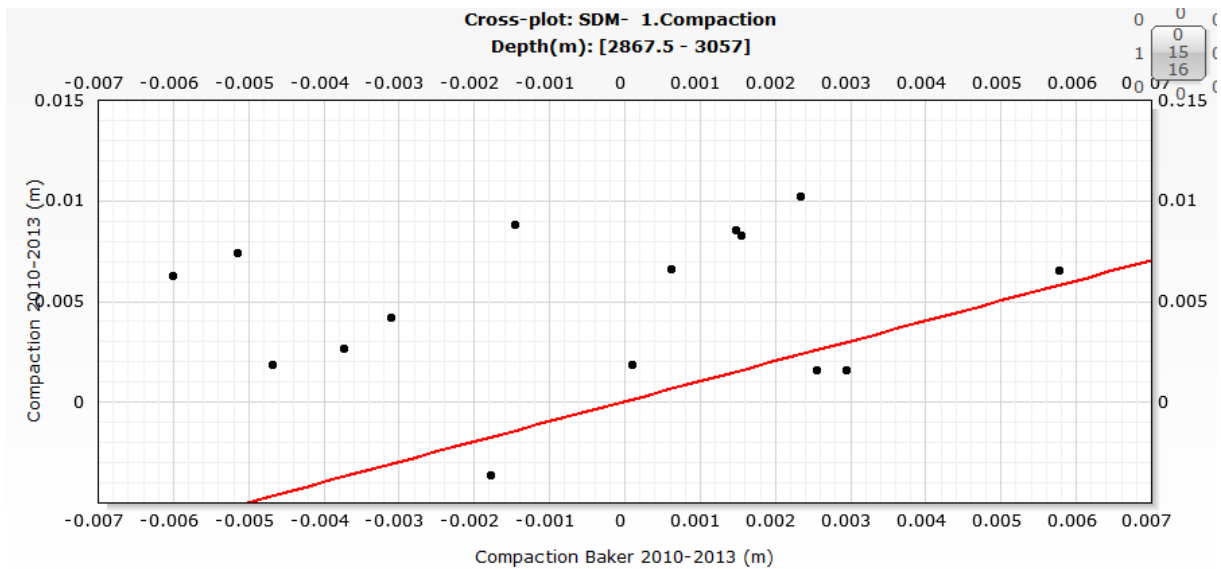


**Figure 17: change of the interval compaction between new interpretation and Baker Hughes interpretation. Red line shows y=x. New analysis shows more compaction, whereas the old interpretation shows a scatter around 0mm.**
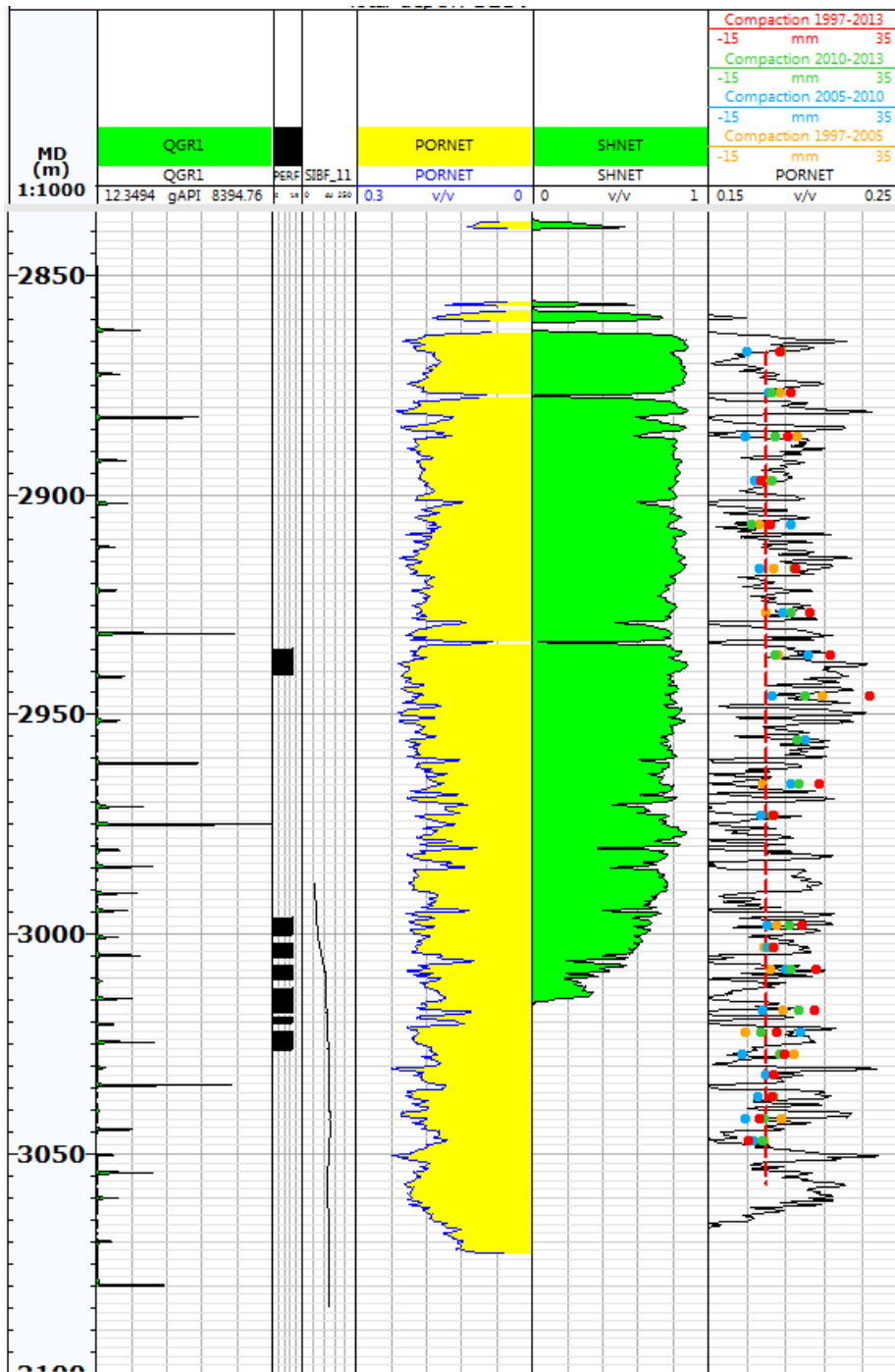
**Figure 18: Successive compaction rates starting in 1997.**
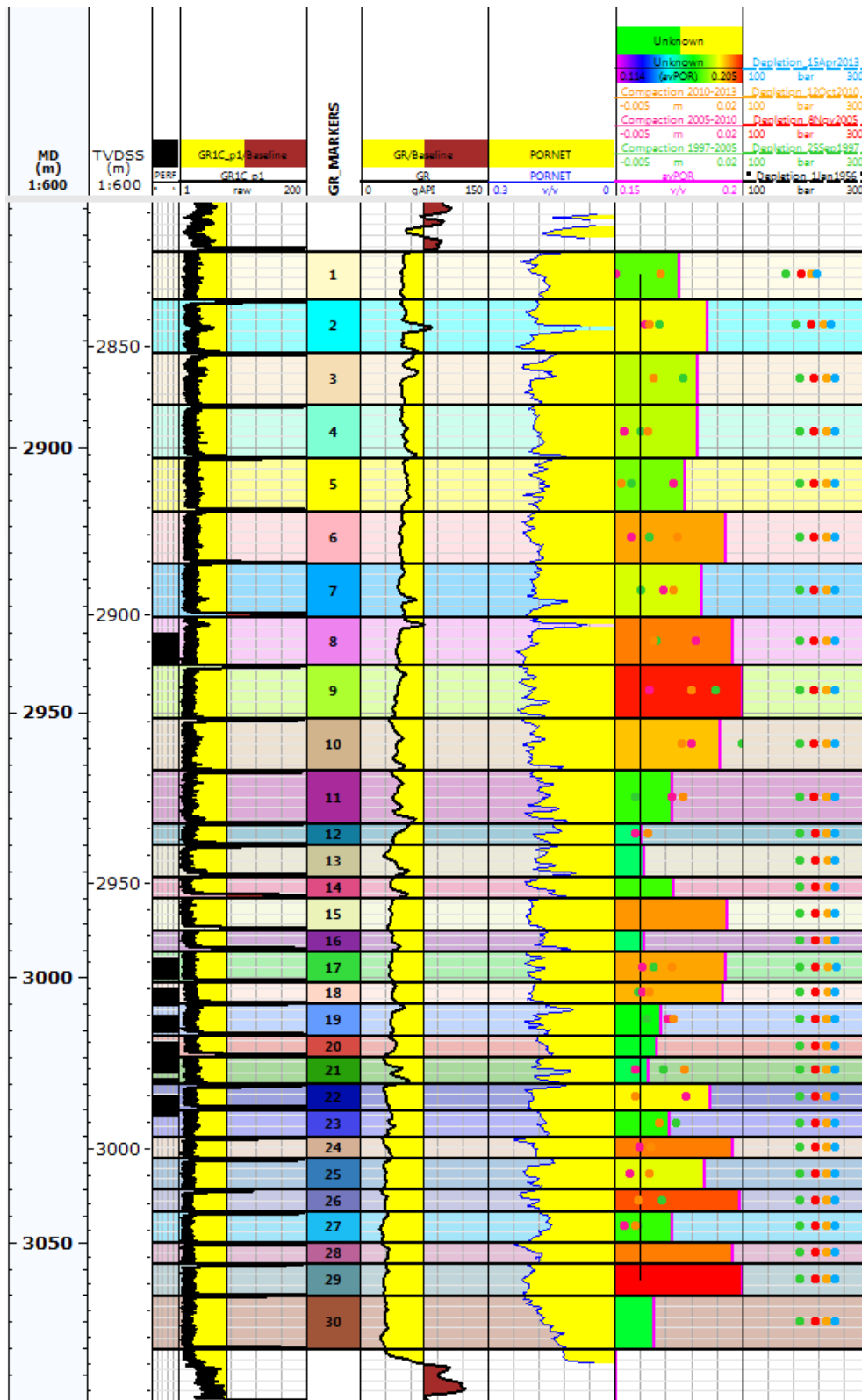
**Figure 19: Compaction and depletion per marker interval**
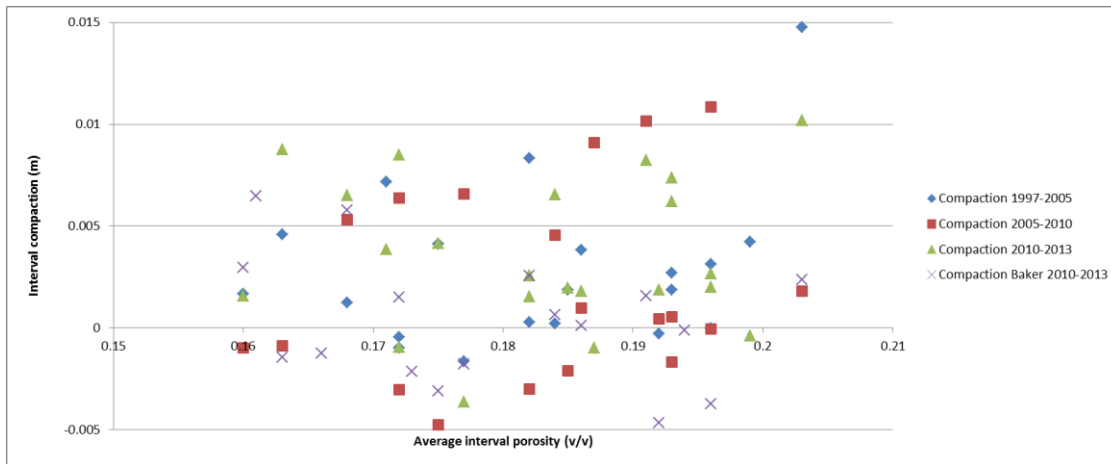
**Figure 20: Interval compaction values compared to average interval porosity.**
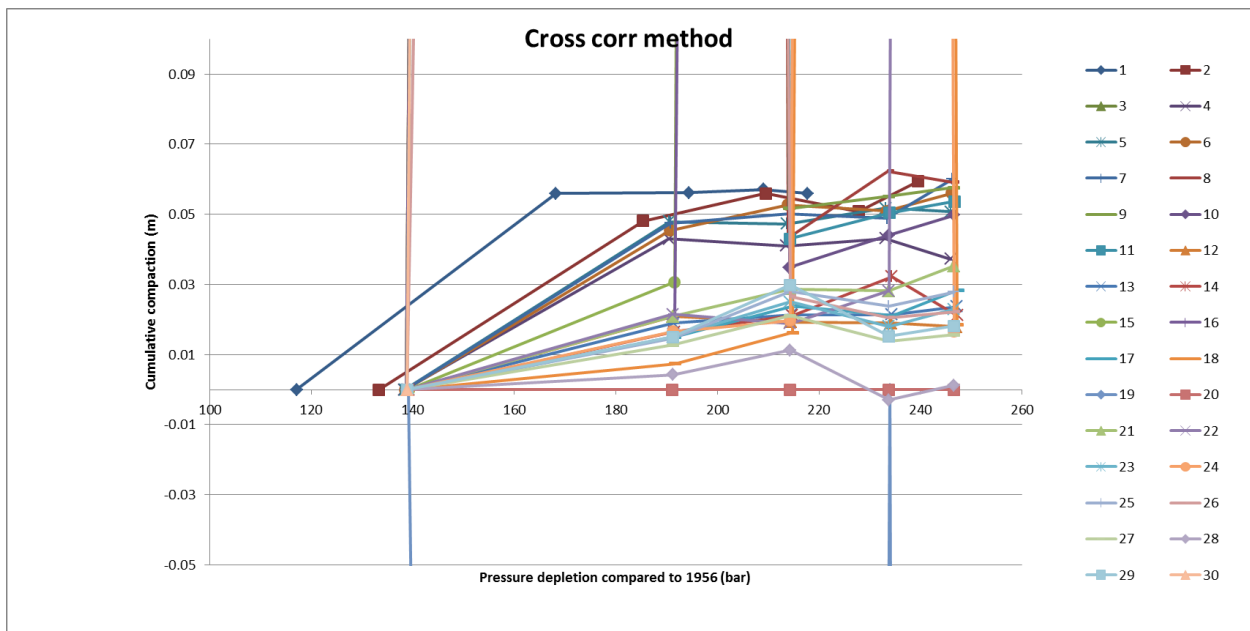


**Figure 21: Cumulative compaction vs pressure depletion for all marker intervals. Earliest data here is from 1986 (lowest depletions in the graph), which is not as reliable due to stick-slip issues.**

# 7   Conclusions

We introduced new methods for analysing the in-situ compaction data from GR markers. One new method is a change of the historical methods, by improving the determination of peak centres. The interval is then simply the difference between two markers, and compaction is determined from the change of these interval lengths with time. A more novel technique is by cross correlating the signals as measured by two different detectors. Unlike the other methods, the cross correlation does not require the detector separation, as it will independently measure the separation, along with the marker separation. The determined detector separation can be compared with the separation measured at surface, and used as a QC of the data. Another QC we get from the cross correlation is

the asymmetry of the resulting signal; if too asymmetric, the data has been affected by stick slip effects, or other unexpected tool motion.

The QC provided by the cross correlation method is very valuable, and not present in the other techniques that obtain marker separations from first determining the actual marker positions. The best one can do in those methods, is rejecting outliers in the data after several runs. Such a QC method, however, will always have data remaining, but will not be able to tell if any of those data are reliable. Systematic changes that occur in all wireline runs, for example, will not be detected.

Simulated signals show that, for data without any unexpected tool movement, the cross correlation method can be accurate to around 1mm, whereas the other two, the improved fit and the historic method, have larger errors, with the historic method giving poorest results with a standard deviation of ~5mm, being larger than that generally quoted. One has to note that on top of this error, errors due to tool movement will be added in the real data. Unreliable data can be removed through QC (easiest QC is from cross correlation method which has several different ways of QC'ing the output), but there will always be some uncertainty on top of that for a perfect signal.

From a theoretical line shape of the marker response, we show that the widths of these peaks are as expected for buried markers. This means that the signal measurement cannot be improved in terms of width by redesigning the logging tools. The only improvement possibly to be made there will be through tool motion control and noise reduction, increased signal to noise.

The methods were applied to the SDM-1 data, where we have the most data (both CMI and FSMT) available. Results from the 1980s are significantly affected by less smooth tool movement. A CMI test was done in 1997 to check different tool string setups. From the QC of the data, it looks like a tool without centralizers has the smoothest movement throughout the wellbore and hence most reliable data.

In general, data around the fluid contact in the wellbore is unreliable due to the buoyancy of the tool, which changes the tension and thereby the actual tool speed. Once the tool is fully submerged in the water, speeds and tensions are constant again, resulting in reliable data. These signatures can be picked up in the cross correlation QC steps.

The emitted gamma ray intensity for $^{137}$Cs halves every 30 years. We show that for most markers the intensity would still be sufficient for determining interval spacing in 60years from now. However, some markers (in SDM-1) already have very little intensity, and these markers will likely drop to a level that makes them unreliable for interval determination.

We now have interval compactions throughout the well bore, which we can compare with the local depletion per interval by importing the pressures from the dynamic reservoir model. This will give a more accurate *Cm* value per interval, as we do not need to use an average pressure depletion of the whole well section. Compaction rates can also be compared to the average porosity per zone.


## 7.1 Outlook

After finalising the analysis of the historic SDM-1 data, we can apply the methods to other wells. First, data from wells HND-1 and ROT-1 will be used as these again have most data coverage. As

these data will likely expose different signal characteristics, they can be used in conjunction with one another to further optimise the workflow.

The accuracy of the GR marker method for compaction monitoring is however not as accurate as more modern techniques that are now available, like the applications of fibre optics for real time compaction monitoring (RTCM). For new fields, it is therefore unlikely that the GR marker technique will be applied in the future.

# 8 References

[1] E. Mobach and H. J. Gussinklo, *In-situ reservoir compaction monitoring in the Groningen field*, SPE 28094, 1994

[2] P. Macini and E. Mesini, *Radioactive marker technique applications to evaluate compaction in environmentally sensitive areas*, SPE 74411, 2002

[3] Internal communiations. Report from 1997 discussing key-wells for in-situ compaction monitoring.

[4] R. Pemper, L. Fjell, R. Gold and F. Ramstad, *Field examples with a new compaction monitoring instrument*, SPWLA 38th annual logging symposium, June 15-18, 1997

[5] Schlumberger analysis presentation

[6] Commonly referred to "G. L. Mathis et al, *Theoretical aspects of compaction monitoring*, technical paper not yet submitted for publication, 1997"

[7] V. I. Ferronsky, *Nuclear Geophysics: applications in hydrology, hydrogeology, engineering geology, agriculture and environmental science*, Springer 2015, data on page 26.

[8] A.J. de Kock, T.J. Johnson, T. Hagiwara, H.A. Zea, F. Santa, *Gulf of Mexico subsidence monitoring project with a new formation compaction monitoring tool*, SPE 52891, SPE Drilling & Completion, 1998

[9] NAM, *Bodemdaling door aardgaswinning, Statusraport 2010 en prognose tot het jaar 2070*, September 2010

# 9  Appendix

Data availability. Tables show the tools run in each year, and the availability of digital (dlis/las/lis format) and print (log print in pdf/tiff). Some data sets have only ASCII tables of interpreted data, which is not suitable for re-interpretation as this requires raw data.

| Well: | **DZL** | | |
|---|---|---|---|
| **Year** | **Tool(s)** | **dlis/las/lis** | **print** |
| 1971 | PDM | | |
| 1972 | PDM | | |
| 1973 | PDM | | |
| 1974 | PDM | | |
| 1975 | | | |
| 1976 | PDM | | |
| 1977 | | | |
| 1978 | PDM | | |
| 1979 | | | |
| 1980 | PDM | | |
| 1981 | | | |
| 1982 | PDM + FSMT | ASCII | |
| 1983 | | | |
| 1984 | FSMT | | |
| 1985 | | | |
| 1986 | | | |
| 1987 | | | |
| 1988 | | | |
| 1989 | | | |
| 1990 | | | |
| 1991 | | | |
| 1992 | | | |
| 1993 | | | |
| 1994 | | | |
| 1995 | FSMT | | |
| 1996 | | | |
| 1997 | | | |
| 1998 | | | |
| 1999 | | | |
| 2000 | | | |
| 2001 | | | |
| 2002 | | | |
| 2003 | | | |
| 2004 | | | |
| 2005 | | | |
| 2006 | | | |
| 2007 | | | |
| 2008 | | | |
| 2009 | | | |
| 2010 | | | |
| 2011 | | | |
| 2012 | | | |
| 2013 | | | |
| 2014 | | | |
| 2015 | | | |

**Figure 22: Data availability in DZL-1**

| Well: | **HND** | Updated 27 Feb 2015 | |
|---|---|---|---|
| **Year** | **Tool(s)** | **dlis/las/lis** | **print** |
| 1971 | | | |
| 1972 | PDM | | |
| 1973 | PDM | | |
| 1974 | | | |
| 1975 | PDM | | |
| 1976 | | | |
| 1977 | PDM | | |
| 1978 | | | |
| 1979 | PDM | | |
| 1980 | | | |
| 1981 | PDM | | |
| 1982 | | | |
| 1983 | FSMT | 🟥 | 🟩 |
| 1984 | | | |
| 1985 | FSMT | 🟥 | 🟩 |
| 1986 | | | |
| 1987 | | | |
| 1988 | FSMT | 🟥 | 🟩 |
| 1989 | | | |
| 1990 | FSMT? | 🟥 | 🟥 |
| 1991 | | | |
| 1992 | | | |
| 1993 | | | |
| 1994 | FSMT | 🟩 | 🟥 |
| 1995 | | | |
| 1996 | | | |
| 1997 | | | |
| 1998 | FSMT | 🟥 | 🟩 |
| 1999 | | | |
| 2000 | | | |
| 2001 | FSMT | 🟥 | 🟩 |
| 2002 | | | |
| 2003 | FSMT | 🟩 | 🟩 |
| 2004 | | | |
| 2005 | | | |
| 2006 | | | |
| 2007 | | | |
| 2008 | | | |
| 2009 | FSMT | 🟩 | 🟩 |
| 2010 | | | |
| 2011 | | | |
| 2012 | | | |
| 2013 | | | |
| 2014 | | | |
| 2015 | | | |

| Well: | **ROT** | Updated 27 Feb 2015 | |
|---|---|---|---|
| **Year** | **Tool(s)** | **dlis/las/lis** | **print** |
| 1971 | | | |
| 1972 | PDM | | |
| 1973 | PDM | | |
| 1974 | PDM | | |
| 1975 | | | |
| 1976 | PDM | | |
| 1977 | | | |
| 1978 | PDM | | |
| 1979 | | | |
| 1980 | PDM | | |
| 1981 | | | |
| 1982 | PDM + FSMT | | |
| 1983 | | | |
| 1984 | FSMT | | |
| 1985 | | | |
| 1986 | FSMT | ASCII | |
| 1987 | | | |
| 1988 | | | |
| 1989 | | | |
| 1990 | | | |
| 1991 | FSMT | | Lots of tiff |
| 1992 | | | |
| 1993 | | | |
| 1994 | FSMT | | |
| 1995 | | | |
| 1996 | FSMT | | |
| 1997 | | | |
| 1998 | | | |
| 1999 | | | |
| 2000 | FSMT | | |
| 2001 | | | |
| 2002 | | | |
| 2003 | | | |
| 2004 | | | |
| 2005 | FSMT | | |
| 2006 | | | |
| 2007 | | | |
| 2008 | | | |
| 2009 | | | |
| 2010 | | | |
| 2011 | CMI + FSM | FSMT and | CMI + FSM |
| 2012 | | | |
| 2013 | | | |
| 2014 | | | |
| 2015 | | | |

| Well: | SDM | Updated 27 Feb 2015 | |
|---|---|---|---|
| **Year** | **Tool(s)** | **dlis/las/lis** | **print** |
| 1971 | | | |
| 1972 | PDM | | |
| 1973 | PDM | | |
| 1974 | PDM | | |
| 1975 | | | |
| 1976 | PDM | | |
| 1977 | | | |
| 1978 | PDM | | |
| 1979 | | | |
| 1980 | PDM | | |
| 1981 | | | |
| 1982 | PDM + FSM | (FSMT only) | March/Ap |
| 1983 | | | |
| 1984 | FSMT | | |
| 1985 | | | |
| 1986 | FSMT | | |
| 1987 | | | |
| 1988 | | | |
| 1989 | | | |
| 1990 | | | |
| 1991 | | | |
| 1992 | | | |
| 1993 | FSMT | **DLIS DATA** | pdf availab |
| 1994 | | | |
| 1995 | **CMI? Print** | REQUESTED | |
| 1996 | | | |
| 1997 | FSMT and | (CMI only) | |
| 1998 | | | |
| 1999 | | | |
| 2000 | FSMT | | |
| 2001 | | | |
| 2002 | | | |
| 2003 | | | |
| 2004 | | | |
| 2005 | FSMT | | |
| 2006 | | | |
| 2007 | | | |
| 2008 | | | |
| 2009 | | | |
| 2010 | CMI | | |
| 2011 | | | |
| 2012 | | | |
| 2013 | CMI | | |
| 2014 | | | |
| 2015 | | | |

| Well: | **TBR** | | |
|---|---|---|---|
| Year | Tool(s) | dlis/las/lis | print |
| 1971 | | | |
| 1972 | | | |
| 1973 | | | |
| 1974 | PDM | | |
| 1975 | | | |
| 1976 | PDM | | |
| 1977 | PDM? | | |
| 1978 | PDM | | |
| 1979 | | | |
| 1980 | PDM | | |
| 1981 | | | |
| 1982 | PDM + FSN | FSMT | |
| 1983 | | | |
| 1984 | FSMT | | |
| 1985 | | | |
| 1986 | FSMT | | |
| 1987 | | | |
| 1988 | FSMT | | |
| 1989 | | | |
| 1990 | | | |
| 1991 | | | |
| 1992 | FSMT | | |
| 1993 | | | |
| 1994 | FSMT | | FSMT 1994 |
| 1995 | FSMT + CN | CMI REQU | CMI tape ( |
| 1996 | | | |
| 1997 | CMI | CMI REQUESTED | |
| 1998 | FSMT | | |
| 1999 | FSMT | FSMT lis | FSMT 1998 |
| 2000 | | | |
| 2001 | | | |
| 2002 | | | |
| 2003 | | | |
| 2004 | | | |
| 2005 | | | |
| 2006 | | | |
| 2007 | | | |
| 2008 | | | |
| 2009 | | | |
| 2010 | | | |
| 2011 | | | |
| 2012 | | | |
| 2013 | | | |
| 2014 | | | |
| 2015 | | | |

| Well: | UHM | | |
|---|---|---|---|
| Year | Tool(s) | dlis/las/lis | print |
| 1971 | PDM | | |
| 1972 | | | |
| 1973 | PDM | | |
| 1974 | | | |
| 1975 | PDM | | |
| 1976 | | | |
| 1977 | PDM | | |
| 1978 | | | |
| 1979 | PDM | | |
| 1980 | | | |
| 1981 | PDM | | |
| 1982 | | | |
| 1983 | FSMT | ASCII | |
| 1984 | | | |
| 1985 | FSMT | ASCII | |
| 1986 | | | |
| 1987 | | | |
| 1988 | | | |
| 1989 | | | |
| 1990 | | | |
| 1991 | | | |
| 1992 | | | |
| 1993 | FSMT | | |
| 1994 | | | |
| 1995 | | | |
| 1996 | | | |
| 1997 | FSMT | | |
| 1998 | | | |
| 1999 | | | |
| 2000 | | | |
| 2001 | | | |
| 2002 | | | |
| 2003 | | | |
| 2004 | | | |
| 2005 | | | |
| 2006 | | | |
| 2007 | | | |
| 2008 | | | |
| 2009 | | | |
| 2010 | | | |
| 2011 | | | |
| 2012 | | | |
| 2013 | | | |
| 2014 | | | |
| 2015 | | | |

| Well: | SPH | | |
|---|---|---|---|
| Year | Tool(s) | dlis/las/lis | print |
| 1971 | PDM | | |
| 1972 | PDM | | |
| 1973 | PDM | | |
| 1974 | | | |
| 1975 | PDM | | |
| 1976 | | | |
| 1977 | PDM | | |
| 1978 | | | |
| 1979 | PDM | | |
| 1980 | | | |
| 1981 | PDM | | |
| 1982 | | | |
| 1983 | FSMT | ASCII | |
| 1984 | | | |
| 1985 | FSMT | ASCII | |
| 1986 | | | |
| 1987 | | | |
| 1988 | | | |
| 1989 | | | |
| 1990 | | | |
| 1991 | | | |
| 1992 | | | |
| 1993 | | | |
| 1994 | | | |
| 1995 | | | |
| 1996 | | | |
| 1997 | | | |
| 1998 | | | |
| 1999 | | | |
| 2000 | | | |
| 2001 | | | |
| 2002 | | | |
| 2003 | | | |
| 2004 | | | |
| 2005 | | | |
| 2006 | | | |
| 2007 | | | |
| 2008 | | | |
| 2009 | | | |
| 2010 | | | |
| 2011 | | | |
| 2012 | | | |
| 2013 | | | |
| 2014 | | | |
| 2015 | | | |

| Well: | SMR | | |
|---|---|---|---|
| Year | Tool(s) | dlis/las/lis | print |
| 1971 | | | |
| 1972 | PDM | | |
| 1973 | PDM | | |
| 1974 | PDM | | |
| 1975 | | | |
| 1976 | PDM | | |
| 1977 | | | |
| 1978 | PDM | | |
| 1979 | | | |
| 1980 | PDM | | |
| 1981 | | | |
| 1982 | PDM + FSM | (FSMT only) | |
| 1983 | | | |
| 1984 | FSMT | ASCII | |
| 1985 | | | |
| 1986 | FSMT | ASCII | |
| 1987 | | | |
| 1988 | | | |
| 1989 | | | |
| 1990 | | | |
| 1991 | | | |
| 1992 | | | |
| 1993 | FSMT | | |
| 1994 | | | |
| 1995 | | | |
| 1996 | FSMT | | |
| 1997 | | | |
| 1998 | | | |
| 1999 | | | |
| 2000 | | | |
| 2001 | | | |
| 2002 | | | |
| 2003 | | | |
| 2004 | | | |
| 2005 | | | |
| 2006 | | | |
| 2007 | | | |
| 2008 | | | |
| 2009 | | | |
| 2010 | | | |
| 2011 | | | |
| 2012 | | | |
| 2013 | | | |
| 2014 | | | |
| 2015 | | | |

| Well: | **USQ** | | |
|---|---|---|---|
| Year | Tool(s) | dlis/las/lis | print |
| 1971 | | | |
| 1972 | | | |
| 1973 | PDM | | |
| 1974 | | | |
| 1975 | | | |
| 1976 | | | |
| 1977 | | | |
| 1978 | | | |
| 1979 | | | |
| 1980 | | | |
| 1981 | | | |
| 1982 | | | |
| 1983 | | | |
| 1984 | | | |
| 1985 | | | |
| 1986 | | | |
| 1987 | | | |
| 1988 | | | |
| 1989 | | | |
| 1990 | | | |
| 1991 | | | |
| 1992 | | | |
| 1993 | | | |
| 1994 | | | |
| 1995 | | | |
| 1996 | | | |
| 1997 | | | |
| 1998 | | | |
| 1999 | | | |
| 2000 | | | |
| 2001 | | | |
| 2002 | | | |
| 2003 | | | |
| 2004 | | | |
| 2005 | | | |
| 2006 | | | |
| 2007 | | | |
| 2008 | | | |
| 2009 | | | |
| 2010 | | | |
| 2011 | | | |
| 2012 | | | |
| 2013 | | | |
| 2014 | | | |
| 2015 | | | |